Master's thesis

NTNU
Norwegian University of Science and Technology
Faculty of Information Technology and Electrical Engineering
Department of Energy and Process Engineering

Karoline Bondø Haug

Strategies for Modelling Dynamic Parameters in Optimization-Based Building Energy Model Calibration: A Case Study

Master's thesis in Energy and Environmental Engineering
Supervisor: Mohamed Hamdy, IBM
June 2019

NTNU
Norwegian University of Science and Technology

Karoline Bondø Haug

Strategies for Modelling Dynamic Parameters in Optimization-Based Building Energy Model Calibration: A Case Study

Master's thesis in Energy and Environmental Engineering
Supervisor: Mohamed Hamdy, IBM
June 2019

Norwegian University of Science and Technology
Faculty of Information Technology and Electrical Engineering
Department of Energy and Process Engineering

NTNU
Norwegian University of
Science and Technology

Abstract

Buildings account for a considerable part of the worlds energy consumption. Although progress has been made concerning the energy requirements for new buildings, it is of great importance to investigate cost-effective solutions for energy diagnosis and retrofitting of the existing building stock. This thesis work explores how different strategies for implementing dynamic parameters in a building energy model affect the calibration of selected building variables. The implications extend to the calibration of building energy models of existing buildings where important parameters like envelope U-values may be unavailable when constructing the energy model.

The chosen case study was Living Lab located in Trondheim. Ten different building energy models were made with varying degrees of hourly scheduled modelling of heat gain sources extracted from measurement data. An optimization-based calibration algorithm was used to compare the indoor air temperature yielded by simulations with the measured temperature. The calibration period was set to two winter weeks, chosen due to the availability of measurement data. The selected calibration variables were the insulation thicknesses in the building envelope, the south window outermost pane conductivity, the infiltration rate and the mechanical ventilation rate. The real values were known beforehand and the discrepancy between the calibration results and the known values were investigated.

It was found that the models with hourly values of dynamic variables extracted from measurement data performed better than the base case with no measurement data used. The findings are qualitative, but underlies the fact that the availability of measurement data is essential for obtaining good calibration results. Building energy model calibration is a key factor in terms of decreasing the performance gap between simulated and measured energy use in buildings. Robust models may contribute to better energy operation, diagnosis and retrofitting of buildings.

Sammendrag

Bygninger står for en høy andel av verdens energiforbruk. Selv om det stadig gjøres fremskritt når det kommer til innstramminger i energikrav for nye bygninger, er det samtidig viktig å undersøke kostnadseffektive løsninger for energieffektivisering av den eksisterende bygningsmassen. Denne masteroppgaven tar for seg hvordan ulike strategier for å implementere dynamiske parametere i en bygningsenergimodell påvirker kalibreringen av et utvalg variabler. Implikasjonene strekker seg til kalibreringen av energimodeller for eksisterende bygg, hvor viktige parametere som blant annet U-verdier kan være ukjente når energimodellen skal konstrueres.

Living Lab lokalisert i Trondheim er valgt som kasusstudie. Ti ulike bygningsenergimodeller ble laget, med en varierende grad av modellering med timesverdier for varmelaster hentet fra måledata. En optimeringsbasert kalibreringsalgoritme ble brukt for å sammenligne simulert innetemperatur med målt innetemperatur. Kalibreringsperioden ble satt til to uker i vinterhalvåret, grunnet tilgangen på måledata fra denne perioden. De utvalgte kalibreringsvariablene var isolasjonstykkelse i bygningskroppen, konduktiviteten i det ytre vindusglasset i de sørvendte vinduene, infiltrasjonsraten og den mekaniske ventileringsraten. De sanne verdiene var kjent på forhånd, og avviket mellom kalibreringsresultater og sanne verdier ble undersøkt.

Det ble funnet at modellene med timesverdier av dynamiske variabler hentet fra måledata ga bedre resultater enn grunnmodellen hvor ingen måledata ble brukt i modelleringen. Funnene er av kvalitativ natur, men bidrar til å fremheve det faktum at tilgjengelighet på måledata er vesentlig for å oppnå gode kalibreringsresultater. Kalibrering av bygningsenergimodeller er en nøkkelfaktor når det kommer til å redusere avviket mellom simulert og målt energiforbruk i bygninger. Robuste modeller vil kunne bidra til en bedring i energieffektiv drift, diagnostisering og oppgradering av bygninger.

Preface

This thesis is the final product of the integrated master study in energy and environmental engineering at NTNU Gløshaugen, Trondheim. It was written during the period of January 2019 to June 2019. The chosen specialization for the five year study has been energy supply and HVAC in buildings.

My interest in reducing building energy use has been present since the start of the study, being the main motivation behind the selection of the engineering specialization. Choosing to enter the field of building energy modelling from an energy-related perspective has allowed me to get familiar with both thermal properties of the building construction, while at the same time offered insight in the heating, ventilation and air-conditioning systems that are key factors when it comes to the building energy performance.

In the fall of 2018 I decided not to go further with the project thesis and changed the theme of my master. In this context I reached out to Mohamed Hamdy, who works as an associate professor at the Department of Civil and Environmental Engineering. Mohamed offered to supervise me in a master thesis about the use of multi-objective optimization to calibrate building energy models. He had co-operated with the PhD-student Sandra Martìnez Mariño in the fall of 2018 to develop an optimization-based genetic calibration algorithm and wanted the algorithm to be tested on a real building. It has been a theoretical approach to solving a practical real-world issue, in which I have enjoyed.

I would like to thank my supervisor Mohamed Hamdy for taking me in as a student even though we belong to different departments. He has been a great support in the process of directing the scope and aim of the thesis. I would also like to thank Sandra Martìnez Mariño for being available for skype meetings and letting me test her calibration algorithm on a real building. Finally I want to thank my co-supervisor Kristian Skeie for helping me find and analyze measurement data from Living Lab, as well as being very helpful and supportive during the process of getting familiar with Living Lab.

Table of Contents

List of Tables

List of Figures

Abbreviations

BEM	=	Building Energy Model
GA	=	Genetic Algorithm
PSO	=	Particle Swarm Optimization
HS	=	Harmony Search
IAQ	=	Indoor Air Quality
ASHRAE	=	American Society of Heating, Refrigerating and Air-Conditioning Engineers
AHU	=	Air Handling Unit
CAV	=	Constant Air Volume
AC/h	=	Air Changes/hour
PCM	=	Phase Changing Material
KPI	=	Key Performance Indicator
NME	=	Normalized Mean Error
NMBE	=	Normalized Mean Bias Error
CV(RMSE)	=	Co-Variation of Root Mean Square Error
SMAPE	=	Symmetric Mean Absolute Percentage Error
MAPE	=	Mean Absolute Percentage Error

Chapter 1

Introduction

1.1 Background and motivation

The concept of anthropogenic climate change has evolved from being a contentious issue to a measurable phenomenon. Energy retrofitting of buildings is an important means of reducing the carbon footprint from the built environment, which contributes to approximately 40% of the greenhouse gas emissions (Global Alliance for Buildings and Construction, 2019). A large share of the existing buildings will still be present for many years to come. In this regard, it is of essence to shed light on the energy refurbishment of this building mass. There is often seen a discrepancy between simulated and measured building energy use. This discrepancy can be explained by uncertainty in the building energy model. This uncertainty may origin from the natural variation of the parameters in the model, or lack of information. Information about envelope parameters are not always present, especially for old buildings that are of particular interest when it comes to energy diagnosis and retrofitting. A strategy for finding these parameters through the use of calibration techniques may contribute to more reliable results, when simulation is used as a tool for investigating various means for improving the energy efficiency of buildings.

1.2 Aim and scope

This thesis explores the calibration of building parameters in the test facility Living Lab in Trondheim, through the use of a multi-objective optimization algorithm developed in Matlab. The inputs of the algorithm are a set of calibration variables, a building energy model and measurement data of a key performance indicator. The optimization algorithm compares the key performance indicator yielded by the simulations with the actual measured performance on an hourly basis. The program alters the calibration variables to minimize the error between the measured and simulated temperatures. The scope is limited to the investigation of how the modelling of dynamic parameters like heating, air conditioning and internal gains affects the outcome of the calibration. 10 different building energy models

were made with different combinations of dynamic parameter modelling. Compensation and cancellation effects resulting from the calibration were investigated. The aim of the thesis is to contribute to a better understanding of how unknown building parameters can be extracted through the use of an optimization-based calibration tool.

1.3 Thesis outline

The first chapter of the thesis is the introduction. The following chapter is a literature review, which starts with a bird's-eye view and narrows down to different strategies for the optimization-based calibration of building energy models. This structure is chosen to contextualize the theme of the thesis and show how it relates to the field of building energy simulation. The next part deals with theory that is used in the methodology part. The fifth chapter introduces the reader to the case study, Living Lab. It is followed by the methodology chapter which describes in a chronological manner the different steps performed to enable the investigation of Living Lab building parameters. In the seventh chapter, the results from the calibration of the building energy models are presented together with a discussion of the results. These parts are merged to avoid repetitive information about the models. Finally the conclusion is presented together with recommendations for future work. The last part of the thesis includes the bibliography and the appendix.

Chapter 2

Problem description

Title: Strategies for Modelling Dynamic Parameters in Optimization-Based Building Energy Model Calibration: A Case Study

The building simulation scope is not limited to building design, but also building operation and diagnosis. Building refurbishment as a means of reducing the energy consumption of the built environment is gaining increased attention. In this regard building energy simulation has proven to be a valuable tool. The increased interest in building monitoring and operation has broadened the possibilities of calibrating building energy models to closely match measured data. The exact values of certain building parameters are not always available for existing buildings. Such unknown parameters can be input calibration variables in an optimization-based algorithm. However, there is a risk that these calibrated values may compensate for other conditions in the model that are the real cause for the discrepancy. The objective of this thesis is to collect building measurement data from a real building and see how the modelling of dynamic variables affects the calibration of selected known variables. The calibration will be performed through the use of a multi-objective optimization algorithm developed in Matlab. Living Lab will be used as a case study due to the access of building information and measurement data. The aim is not limited to the calibration of Living Lab, but to explore results that may be applicable to other buildings and hereby relevant to the building industry in general.

Supervisor: Mohamed Hamdy, *Associate Professor, Department of Civil and Environmental Engineering, NTNU*
Co-supervisor: Kristian Stenerud Skeie, *PhD Candidate, Department of Architecture and Technology, NTNU*

Chapter 3

Literature Review

This chapter deals with a literature review of building performance simulation and contextualizes building energy model calibration. Furthermore it provides a brief overview of some of the optimization-based calibration techniques that are seen today. The subchapters about building performance simulation and uncertainty analysis are collected from the project thesis *Energy-related occupant behavior - Movement monitoring*, written by the author (Haug, 2018).

3.1 Performance based buildings

One of the big challenges in today's building sector is to design sustainable buildings that also fulfill the operational requirements that the building is intended for (Hensen and Lamberts, 2011). The challenge is complex due to the many dynamic processes to take into account, with some of them being potentially conflicting. The interactions are illustrated in figure 3.1. The rise of global temperatures and human contribution to climate change is one key factor that urges regulations towards the building industry in reducing both energy use in construction processes, together with the recycling of materials and the usage of materials with reduced carbon footprints. Another aspect is the operational energy use of the building. The annual energy use must be within certain limits set by national authorities. At the same time, building usage has become more flexible with the introduction of technology that facilitates work out of office and other changing occupancy patterns. The technology has also contributed to growing occupant demands and expectations of comfort. The link between indoor environment and productivity, well-being and health of the occupants is also gaining increasing attention. To enable the simultaneous management of all these aspects, an integrated approach is required in order to achieve robust building and system solutions (Claridge, 2011).

Traditionally, buildings have been designed by the means of prescriptive terms. The various properties of a building have been the key design parameters, not the actual performance of the building (Augenbroe, 2011). A simple example is the focus on facade U-values, thermal bridges and infiltration as opposed to the buildings' annual energy use

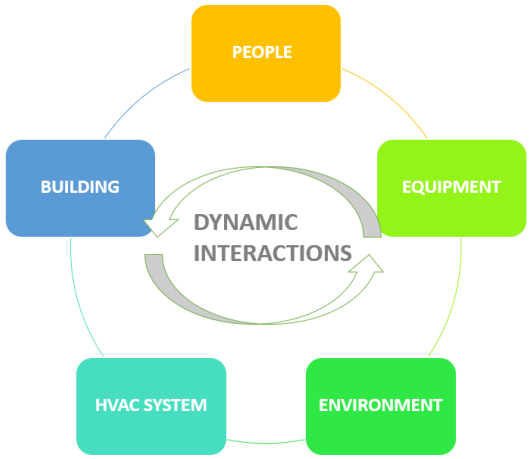

Figure 3.1: Building subsystems (Hensen and Lamberts, 2011)

for heating and cooling. They are indeed related, however the focus on performance indicators such as annual energy use, indoor temperatures and indoor air quality as design parameters themselves has not been the main driving force in building design. The increasing complexity of building performance simulation enables a more detailed analysis of these key performance indicators (KPI).

3.2 Building performance simulation

Building Performance Simulation (BPS) consists of using software to simulate different aspects of building performance. The analysis of energy consumption represents a challenging task, due to the complex interaction between the building, climate and weather, occupants, HVAC system among other subsystems like electrical equipment (Mustafaraj et al., 2014). Numerous programs like EnergyPlus, ESP-R and IDA-ICE have been developed to investigate the energy demand and indoor air quality (IAQ) of buildings. The simulation tools usually include apprehensive databases with information regarding weather data from the geographical areas the simulations are intended for, solar intensity throughout the year and daylight availability. When modelling the building, the software prompts the user for input data, like the geometry, orientation, material specifications, infiltration and domestic hot water use among other parameters. Depending on the program, a simplified or detailed HVAC system and scheduling of lighting, equipment and occupancy may also be implemented. Based upon the collected information, predictions regarding the annual energy demand is calculated by the software. However, the discrepancy between predicted building performance and the simulated building performance, is found to be considerable (Khoury et al., 2017). The discrepancy can be explained by doing an uncertainty analysis of the simulation process.

3.3 Uncertainty analysis

For every modelling process where computation is utilized to simulate a physical system, there are numerous choices to be made which affects accuracy in predictions. Both the software developers and the user of the software impact how well the simulations represents reality (National Research Council, 2012). Some of the information implemented in computational models may lack the benefit of precision, others may be influenced by various assumptions that has to be done. When adding up all of the potential uncertainty factors, the simulation process has the potential of falling victim to serious validity concerns. On a general basis, the uncertainty in building energy models can be divided into two main categories, depending on the order of which data is obtained and analyzed (Tian et al., 2018). Figure 3.2 illustrates the two categories.

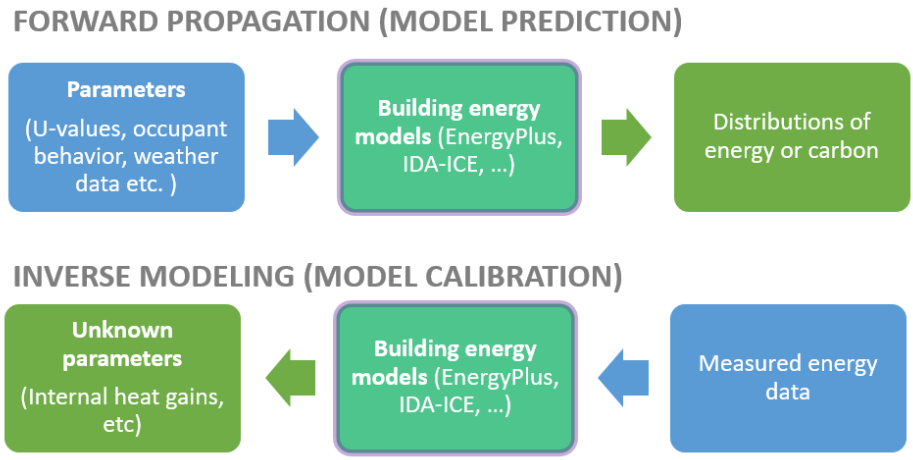

Figure 3.2: Forward and inverse data uncertainty analysis in building performance analysis (Tian et al., 2018)

The software simulations represent a forward uncertainty propagation. The input parameters are being used in mathematical models to quantify the system uncertainty, generated by the uncertainty of the individual parameters. In model calibration, measured energy data from buildings are used for determining the unknown variables with the use of mathematical models. The uncertainty in forward propagation is the most studied, even though both uncertainty factors are present in terms of building performance analysis. This may be due to the fact that the uncertainty quantification in model calibration represents more difficulty. Nevertheless, they are closely linked. To enable the determination of uncertainty in parameters, the results from the inverse uncertainty analysis in the measured energy data can be used for energy predictions from various energy saving methods (Heo et al., 2012). When dealing with computational modelling, a distinction between two sources of uncertainty is often made. One source is called the epistemic uncertainty. This category represents the systematic uncertainty caused by a lack of knowledge of the physical system. The other source, aleatory uncertainty, represents the uncertainty that comes

with the natural variation of the physical system that is being modelled (He et al., 2015).

3.4 Calibration of building energy models

Calibration can be used as a means to reduce systematic uncertainty in building performance simulation. This process consists of using an existing building simulation software and ”tuning”, or calibrating, the inputs so that observed energy use matches with the energy use predicted by the software (Reddy, 2006). This calibration process relies on the access of measured building data. There are several motivations for calibrating a building energy model. One is to identify potential building energy savings and demand reduction measures. Another is to identify parts of the building that will benefit from further analysis (Ramos Ruiz et al., 2016). Calibration also increases the confidence in further simulations. There are several ways of approaching the calibration process. Mustafaraj et al. (2014) identifies three general methods:

1. *Iterative*. The calibration is done manually by the user with a trial-and-error approach. The method relies heavily on the user's experience with building energy simulation.

2. *Graphical*. Graphical representations of outputs offered by the simulation runs are compared with measured data. Comparison of for instance peak loads or temperature profiles are used to further orient the calibration.

3. *Automated methods*. The calibration is done in an automated manner, by the use of a calibration software. This may be performed with a multi-objective optimization tool which adjusts certain parameters and compares simulation outputs with measured data.

3.4.1 Optimization-based calibration

There have been developed many tools to investigate the trade-off between competitive objectives. The optimization approach is typical for engineering processes in the design phase, where contrasting objectives are compared to reach the optimal solution. More recently, this optimization-based approach has entered the field of building energy model calibration (Lara et al., 2017). Typically, a brute-force approach has been used where all possible options are investigated by performing sensitivity analyses with parametric studies. This approach is often computationally expensive and time-consuming. For this reason, optimization-based algorithms have been implemented to speed up the calibration process. The following text identifies three strategies that are commonly seen in optimization-based building energy model calibration.

Genetic algorithm

Genetic algorithms (GA) have been found to be effective for the investigation of calibration parameters. GA is based on the theory of evolution by Darwin. The algorithm starts with an initial population of random individuals, in this instance, sets of random values

for the calibration variables within specified upper and lower bounds. Each individual solution is treated as a chromosome, containing a number of variables, or genes. The chromosomes with the best scores from the initial generation are further selected to create the next generation. This is done by either altering the genes from the different solutions, called cross-over, or introducing random changes, called mutation. The algorithm may be stopped by either defining a number of suitable solutions to look for, or a maximum number of generations allowed. Figure 3.3 illustrates the process. This genetic algorithm function is available in the *Matlab Global Optimization Toolbox* and lays the foundation of the optimization-based algorithm used in this thesis. In a study by Lara et al. (2017), both a parametric approach and a genetic algorithm approach were used to calibrate the High School State Institute Francesco da Collo in Conegliano Veneto. It was found that the parametric calibration took 4746 calculation hours, whereas the genetic algorithm spent 90 calculation hours to achieve a similar Pareto frontier with optimal solutions.

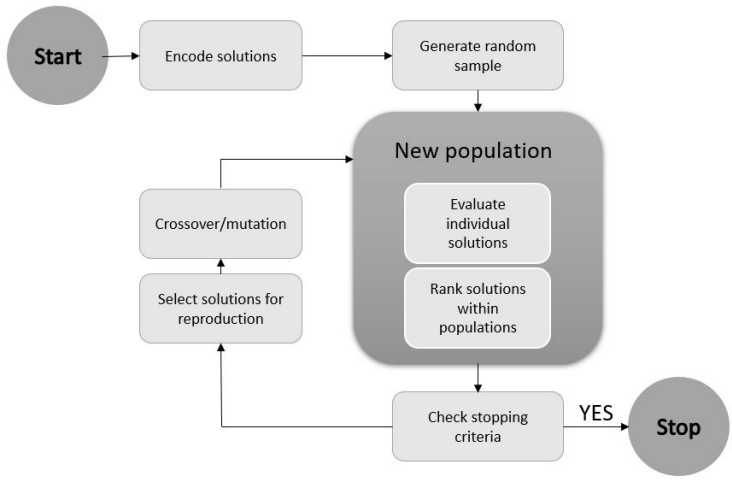

Figure 3.3: Genetic algorithm procedure (Lara et al., 2017)

Particle Swarm algorithm

Particle Swarm Optimization (PSO) has taken inspiration from the synchronous, social interaction of bird flocks and fish schools. The methodology was created by Kennedy and Eberhart (1995) as a means of optimizing nonlinear functions. The algorithm introduces a population of particles, namely a swarm, which is capable of adjusting their time dependent position based on information about their own and their neighbouring particles' position (Slanzi et al., 2014). The velocity of each particle is adaptable and the best position it has visited is recorded. The best position transfers to the position with the lowest objective function value. In building energy model calibration, this signifies the position with the lowest discrepancy between simulated and measured data. The optimal positions by the neighborhood particles are communicated with each other and affect the movement of the individual particles, referred to as the social component. The cognitive component

is the particle's recognition of its own best position. The optimal solution is reached when the neighborhood of each particle consists of the whole swarm, yielding a continuous connection among the particles.

In a case study by Monetti et al. (2015), particle swarm optimization was used for calibrating a building energy model. The key performance indicator used for calibrating the parameters was the building heating energy consumption. Occupancy was not considered as it was a test facility. The parameters were altered within a specified upper and lower bound until the simulated heating consumption closely matched the monitored heating consumption. The methodology was centered around four steps. Step 1 was the creation of an uncalibrated building energy model in the software EnergyPlus. Step 2 was pre-processing, where data regarding heating consumption and weather information was collected. An optimization tool, GenOpt, was coupled with the uncalibrated EnergyPlus building energy model. The calibration parameters were selected based on a literature review of uncertainty within building energy models and further given upper and lower bounds for calibration. In step 3, the optimization was performed. The strategy used was a hybrid pattern search with particle swarm optimization. Step 4 included post-processing where the outputs were tested for accuracy through the use of Mean Bias Error (MBE), the Root Mean Square Error (RMSE) and the Coefficient of Variation of RMSE (CV(RMSE)). It was found that the calibration of static building envelope parameters performed better than the calibration of time dependent parameters like internal gains, ground temperature and infiltration rates. ASHRAE Guide 14 considers a building model calibrated if hourly MBE values fall within $\pm 10\%$ and hourly CV(RMSE) values fall below 30% (Garrett and New, 2016). All of the models reached the MBE treshold after 11 calibration runs.

Harmony Search algorithm

Another optimization-based calibration approach is the use of the harmony search (HS) algorithm. The method was developed by Geem and Kim (2001) and is illustrated in figure 3.4. It has proven to be a powerful tool for building energy model calibration (Asadi et al., 2019). The method is based on heuristic principles and mimicks the improvisation of music players (Geem and Kim, 2001). The key element of the algorithm is the combination of both rules and and randomness, to achieve an optimization strategy that imitates natural phenomena. There are four steps in the process. Step 1 is the initialization of a harmony memory. In figure 3.4 it is illustrated by the initial random solution. In step 2, a new harmony is improvised from harmony memory, which is transferable to the process of simulation. Step 3 involves the testing of the harmony memory, or simulation result. If the result is better than the previous, it is stored in memory. The least optimal result previously stored is then excluded from memory. Step 4 is the progress back to step 2 if the stopping criteria are not satisfied.

The literature review has revealed that there are many ways of implementing optimization-based algorithms for the calibration of building energy models, as opposed to a unique, global standard. Every calibration process is a function of available resources, like computational power, the complexity, aim and scope of the task as well as the previous experience of the building energy modeller.

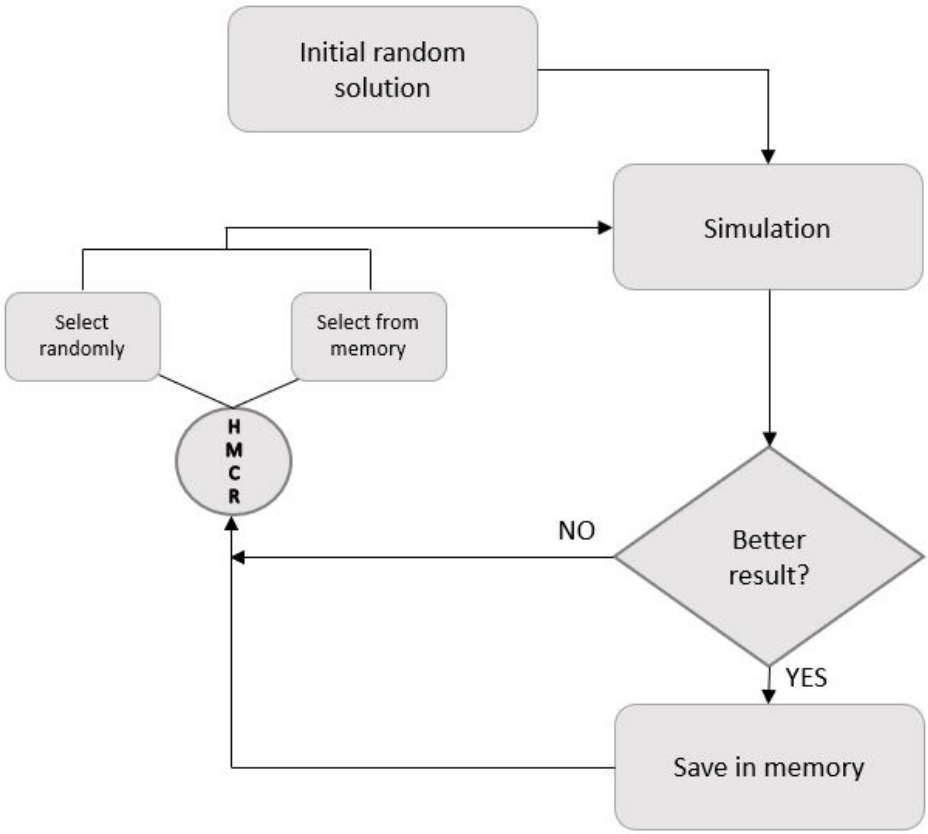

Figure 3.4: Harmony search algorithm procedure (Asadi et al., 2019)

Chapter 4

Theory

The following chapter includes theory that is considered relevant for the understanding of the simulation and calibration processes presented in the thesis. The error estimation chapter sheds a light on the mathematical foundation behind the objective functions in the calibration algorithm. The heat transfer parts elaborates on thermodynamic properties of the calibration variables and the building energy model.

4.1 Error estimation

To enable the calibration of a model, the error between measured and simulated data must be taken into account. There are many approaches when it comes to calculating this error. In its simplest form, the error is found by equation 4.1:

$$\epsilon = M_i - S_i \tag{4.1}$$

where:
M_i = measured data at instance i
S_i = simulated data at instance i

The following subchapters deal with the five error estimation methods used in the calibration algorithm, as well as the SMAPE indicator used for evaluating the resulting calibrated variables.

4.1.1 Normalized Mean Error

The Normalized Mean Error (NME) is a dimensionless indicator that sums the absolute difference between the measured and simulated results for the same time interval, and divides it with the total of the measured data values (Ruiz and Bandera, 2017).

$$NME = \frac{\sum_{i=1}^{n} \mid M_i - S_i \mid}{\sum_{i=1}^{n} M_i} \times 100 \tag{4.2}$$

4.1.2 Normalized Mean Bias Error

The Normalized Mean Bias Error (NMBE) gives the global difference between the simulated and real values. A shortcoming when it comes to the NMBE indicator is the potential cancellation effect. A negative value indicates that the simulated value is an underprediction, whereas a positive value is an indication of a simulated over-prediction. The sum of these values can lead to a good NMBE score, although the model may suffer from validity concerns.

$$NMBE = \frac{\sum_{i=1}^{n} (M_i - S_i)}{\sum_{i=1}^{n} M_i} \times 100 \tag{4.3}$$

4.1.3 Coefficient of Variation of Root Mean Square Error

The next dimensionless error estimation equation shares similarities with 4.1.2, with the exception being that the difference between measured and simulated data is squared, followed by a root after the sum is iterated through. This leaves out potential cancellation effects (Royapoor and Roskilly, 2015).

$$CV(MRSE) = \frac{1}{\bar{M}} \cdot \sqrt{\frac{\sum_{i=1}^{n} (M_i - S_i)^2}{n}} \times 100 \tag{4.4}$$

4.1.4 Coefficient of determination ($\mathbf{R}^2$)

The coefficient of determination, R^2, is a measure of how much of the variation in a dependent variable that can be explained by the independent variable. The method implies a graphical approach, where the closeness of the simulated values compared to the regression line of the measured values is calculated. A coefficient of determination value of 1 indicates a perfect match between measured and simulated values. On the other hand, a low value indicates big differences between the simulated and the measured values. The American Society of Heating, Refrigerating and A-C Engineers (ASHRAE) recommends that the obtained R^2- value should never be less than 0.75 for calibrated models (Ruiz and Bandera, 2017).

$$R^2 = \left(\frac{n \cdot \sum_{i=1}^{n} M_i \cdot S_i - \sum_{i=1}^{n} M_i \cdot \sum_{i=1}^{n} S_i}{\sqrt{(n \cdot \sum_{i=1}^{n} M_i^2 - (\sum_{i=1}^{n} M_i)^2) \cdot (n \cdot \sum_{i=1}^{n} S_i^2 - (\sum_{i=1}^{n} S_i)^2)}} \right)^2 \tag{4.5}$$

4.1.5 Standardized Contingency Coefficient

The standardized contingency coefficient, C_{χ^2}, is based on the chi-squared test (Vogt et al., 2018). This test is frequently used in statistics to evaluate the dependency between simulated and measured data. Firstly, The hourly difference δy_t between the data is calculated and categorized in three categories:

1: $\Delta y_t > 0$: increasing value
2: $\Delta y_t < 0$: decreasing value
3: $\Delta y_t = 0$: constant value ($\pm 1.5\%$)

Secondly, the contingency table shown in table 4.1 is derived from the categorization. N indicates the total number of intervals Δy_t, whereas N^{obs} and N^{exp} indicates the observed and expected numbers of occurrences of a certain interval y_t, respectively.

Table 4.1: 3x3 contingency table for χ^2-test

		Measurement			
		decrease	constant	increase	Total
Simulation	decrease	$N_{1,1}^{obs}$	$N_{1,2}^{obs}$	$N_{1,3}^{obs}$	N_1
	constant	$N_{2,1}^{obs}$	$N_{2,2}^{obs}$	$N_{2,3}^{obs}$	N_2
	increase	$N_{3,1}^{obs}$	$N_{3,2}^{obs}$	$N_{3,3}^{obs}$	N_2
	Total	N_1	N_2	N_3	N

The chi-square statistic tests the statistical dependency between the simulated and measured data, and may be calculated with equation 4.6:

$$\chi^2 = \sum_{k=1}^{3} \sum_{j=1}^{3} \frac{(N_{k,j}^{obs} - N_{k,j}^{exp})^2}{N_{k,j}^{exp}} \tag{4.6}$$

where:
$N_{k,j}^{exp} = \frac{N_k \cdot N_j}{N}$

The chi-square statistic decreases when the observed number $N_{k,j}^{obs}$ is a good match to the expected number $N_{k,j}^{exp}$. This signifies that the observed distribution fits the theoretical distribution and indicates that the corresponding distribution is random. Hence, a great χ^2-value increases the likelihood of a dependency between the simulated and measured data. The standardized contingency coefficient is a means of limiting the range of the coefficient from $0 - 1$:

$$C_{\chi^2} = \sqrt{\frac{m}{m-1}} \cdot \sqrt{\frac{\chi^2}{N + \chi^2}} \tag{4.7}$$

where:
χ^2 = the chi-square statistic

N = the total number of data points/measurements
C_{χ^2} = the standardized contingency coefficient
m = number of rows/columns in the contingency table = 3

A C_{χ^2} close to 1 indicates a strong association between measured and simulated data, whereas a C_{χ^2} close to zero indicates a low degree of association.

4.1.6 Symmetric Mean Absolute Percentage Error

The symmetric mean absolute percentage error, or SMAPE, may be used as an indicator for the comparison of calibration outcomes against the real values for calibration parameters.

$$\frac{100}{n}\sum_{i=1}^{n}\frac{\mid F_i - A_i \mid}{\frac{|F_i|+|A_i|}{2}} \tag{4.8}$$

where:
n = number of parameters
F_i = calibrated parameter value
A_i = known parameter value

4.2 Heat transfer

The heat transfer between the building envelope and the surroundings is fundamental when it comes to analyzing the building performance. Heat transfer may be described by three different processes, namely conduction, convection and radiation (Rajendra, 2017).

4.2.1 Conduction

Conduction implies heat transfer through a material. The particles in the body transfer heat without the need of motion of the material. Whenever a temperature gradient exists in a media, thermal conduction occurs. The one-dimensional, steady-state transfer of heat through conduction is described by the Fourier equation:

$$\dot{q} = -kA\frac{dT}{dx}\,[W] \tag{4.9}$$

where:
$\dot{\mathrm{q}}$ = heat transfer rate (W)
k = thermal conductivity (W/mK)
A = area normal to the heat flow (m^2)
$\frac{\mathrm{dT}}{\mathrm{dx}}$ = temperature gradient (K/m)

Most building envelope constructions consist of more than one layer. By defining a thermal resistance R for each layer, the total resistance can be summarized and hereby the total convection heat transfer.

$$R = \frac{x_2 - x_1}{k} = \frac{\Delta x}{k} \ [m^2K/W] \tag{4.10}$$

where:
Δx = layer thickness (m)

$$\sum_{i=1}^{n} R_{tot} = R_1 + R_2 + ... + R_n \tag{4.11}$$

The one-dimensional steady state conduction heat transfer can then be modelled by equation 4.12.

$$\dot{q} = A\frac{T_1 - T_2}{R_{tot}} \ [W] \tag{4.12}$$

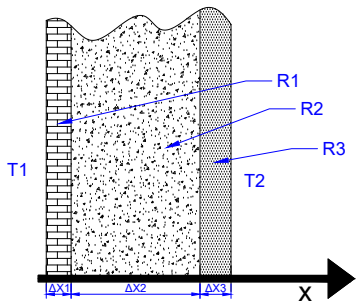

Figure 4.1: One-dimensional conduction through a wall

4.2.2 Convection

Heat transfer by convection implies movement of the medium itself (Rajendra, 2017). Convection happens when a fluid moves from a region of one temperature state to another region with another temperature. Fluid may refer to both gases and liquids. When cold air meets a warm surface, the surface heats up the surrounding air and causes the density of air to decrease. This will in turn cause the denser air to move towards the warmer air near the surface due to pressure differences. The movement caused by temperature differences and the gravitational force are referred to as convection currents. The effect is called buoyancy and the convection flow is referred to as natural convection. The forced movement of a liquid through the use of a fan or other mechanical equipment is referred to as forced

convection. The heat transfer between a solid surface and a fluid can be described by Newtons law of cooling:

$$\dot{q} = hA\Delta T \, [W] \tag{4.13}$$

where:
h = heat transfer coefficient ($\mathrm{W/m^2K}$)
A = surface area ($\mathrm{m^2}$)
ΔT = temperature difference between solid and bulk fluid (K)

4.2.3 Radiation

Radiation heat transfer is the transfer of thermal energy by electromagnetic waves (Spitler, 2011). A body emits a certain amount of energy by radiation, which depends on the temperature and the emissivity ϵ of the body. Radiation is not dependent on any liquid or solid material, hence it may exist in a vacuum. The thermal energy radiates from one surface and is absorbed by another surface. The amount of energy that is absorbed, emitted or reflected by a surface will depend on wavelength and the relative direction of the radiation with regards to the surface. The direction dependency is called *specular*. Some surfaces are not dependent on the direction of the radiation, and they are referred to as *diffuse*. Surfaces that are dependent on the wavelength are called *spectral*, whereas surfaces independent on the wavelength are called *grey*. Important parameters when it comes to radiation are:

- Absorptance α, the ratio of radiation that is absorbed by the surface. A *blackbody* absorbs by definition all the radiation incident on it.
- Emittance ϵ, the ratio of radiation that is emitted by a surface compared to a blackbody with an equal temperature.
- Reflectance ρ, the ratio of radiation that is reflected by a surface to that incident on the surface.
- Transmittance τ, the radiation ratio transmitted by a translucent surface to that incident on the surface.

With relevance to building physics, most surfaces are treated as gray and diffuse. However, Spitler (2011) accounts for two exceptions. The first one is the distinction between the short-wave radiation and the long-wave radiation emitted by internal gains in the building, such as occupants and lighting. The second exception is for windows, where solar radiation may be treated either as specular or diffuse. Since the solar beam angles are of importance for the thermal radiation through the windows, they are generally hourly calculated for the specific incidence angle. Radiation heat transfer between surface 1 and surface 2 may be calculated using equation 4.14.

$$\dot{q}_{1-2} = \frac{\sigma(T_1^4 - T_2^4)}{\frac{1-\epsilon_1}{A_1\epsilon_1} + \frac{1}{A_1 F_{1-2}} + \frac{1-\epsilon_2}{A_2\epsilon_2}} \tag{4.14}$$

where:
σ = Stefan-Boltzmann constant (5.673 $\cdot 10^{-8} (\mathrm{W/m^2K^4})$
T_1 and T_2 = surface temperatures of surface 1 and 2 (K)
ϵ_1 and ϵ_2 = emittances of surface 1 and 2
F_{1-2} = View factor from surface 1 to surface 2

Irradiation

Irradiation is an expression that describes how much radiation that is received by a surface. For building energy modelling, the solar irradiation is an important variable in terms of the solar thermal gains. *Direct normal irradiation* is a measure of the solar radiation that is received per unit area of a surface that is always perpendicular to the solar rays (Bird and Riordan, 2002). The direct normal irradiation is hence a function of the solar position. Equation 4.15 may be used for calculation.

$$I_{d\lambda} = H_{o\lambda} \cdot D \cdot T_{r\lambda} \cdot T_{a\lambda} \cdot T_{w\lambda} \cdot T_{o\lambda} \cdot T_{u\lambda} \tag{4.15}$$

where:
$H_{o\lambda}$ = extraterrestrial irradiance at the mean earth-sun distance for wavelength λ
D = correction factor for the earth-sun distance
$T_{r\lambda},\ T_{a\lambda},\ T_{w\lambda},\ T_{o\lambda},\ T_{u\lambda}$ = transmittance functions of the atmosphere at wavelength λ for molecular scattering, aerosol attenuation, water wapor absorption, ozone absorption and uniformly mixed gas absorption, respectively.

Diffuse horizontal irradiation takes into account the scattering by atmospheric molecules and particles, describing the amount of radiation that is received per unit area of a surface that has been obstructed by clouds and other weather conditions. When investigating the effect of solar radiation in terms of building energy models or photovoltaic panels, it is the diffuse irradiation that is most relevant, given the fact that clouding is an important variable. There are numerous ways of approaching the calculation of diffuse horizontal radiation, which will not be elaborated upon in this thesis.

4.3 U-values

In building physics, thermal transmittance, often referred to as the U-value, is a measure of the steady-state heat transfer through a building envelope component (Ferrari and Zanotto, 2016). The U-value takes into account the internal and external heat transfer coefficients, $h_{s,i}$ and $h_{s,o}$, as well as the conduction heat transfer through the component as described in chapter 4.2.1. The heat transfer coefficients are dependent on wind, temperature and pressure differences on the inner and outer surface of the component. When these coefficients are found, together with the overall thermal resistance of the wall given by equation 4.11, the U-value can be found by the following equation:

$$U = R_{s,i} + R_{tot,wall} + R_{s,o} = (\frac{1}{h_{s,i}} + R_{tot,wall} + \frac{1}{h_{s,o}})^{-1}\ [W/m^2K] \tag{4.16}$$

There are reference values for $h_{s,i}$ and $h_{s,o}$ that can be found in the standard *ISO-6946:2017*, which also is adopted and used as the Norwegian Standard.

4.4 Thermal bridges

It is inevitable to avoid areas of increased heat flow in building constructions (Waters, 2003). These areas are referred to as thermal bridges. Among other reasons, they most commonly appear in insulation gaps or junctions caused by the building structure and geometry, or due to damages in the insulating material. In winter, the increased amount of heat leaving the building envelope at the point of the thermal bridge leads to a lower inside surface temperature and a higher outside surface temperature. The elevated surface temperature enables the detection of thermal bridges through the use of infrared cameras.

When the U-value requirements for building envelope constructions decreases, the percentage of thermal losses caused by thermal bridges increases. The detection and calculation of thermal bridges is important when evaluating the energy performance of a building. It may be calculated as either linear or point transmittances. A normalized thermal bridge value is most common seen in simulation software. Point transmittance is often neglected due to complexity. The linear thermal transmittance is represented by Ψ, and can be found tabulated in *UNI-EN ISO 14683:2008* for different material- and geometry combinations. The calculation of Ψ can otherwise be done by the use of formula 4.17:

$$\Psi = L_{2D} - \sum_{j=1}^{N_j} U_j l j \ \ [W/K] \tag{4.17}$$

where:

L_{2D} is the thermal coupling coefficient obtained from a 2D-calculation of the component separating the two environments being considered [1]

U_j is the thermal transmittance over the 1D-component, *j*, separating the two environments being considered

l_j is the length over which the value U_j applies

[1] See ISO10211:2017 for a detailed instruction on how to calculate this coefficient

Chapter 5

Case Study

5.1 ZEB Living Lab, NTNU

The building selected for the testing of the optimization algorithm is the NTNU Living Lab, located in Trondheim, Norway. The building was designed by the Research Centre on Zero Emission Buildings at NTNU and the construction process was finished in 2015. The facility resembles a single-family house. It was built to enable energy-related investigation and scientific analysis. Both envelope components, HVAC control strategies, research on occupant behavior and the interaction between occupants and ZEB buildings was the aim of the construction (Goia et al., 2015). The building envelope and technical installations in the building are thoroughly documented, which increases the input accuracy in energy simulations. The building is also extensively equipped with energy sensors, facilitating calibration and validation of the simulation outputs.

The Living Lab has a heated surface floor area of $104\ m^2$, yielding a gross volume of approximately $350\ m^3$. There is an open-space solution with no internal partitions between the kitchen and living room area. Living Lab contains two bedrooms, located at the northwest and northeast corners of the building. Figure 5.2 shows the floor plan with zoning.

5.1.1 Building specifications

Table 5.1 gives information about the layers and average U-values of the different parts of the construction.

More detailed specifications concerning the material layers in the roof, floor, walls and windows were found in the article *Life Cycle GHG Emissions of Material Use in the Living Laboratory* (Wiik, 2017) and by investigation the presentation *Living Lab - A ZEB-pilot project at NTNU* (Carlucci, 2019). Table 5.2 is an example of the construction details taken from the presentation.

Figure 5.1: Living Lab at NTNU, Trondheim (NTNU Department of Archtecture and Technology, 2019)

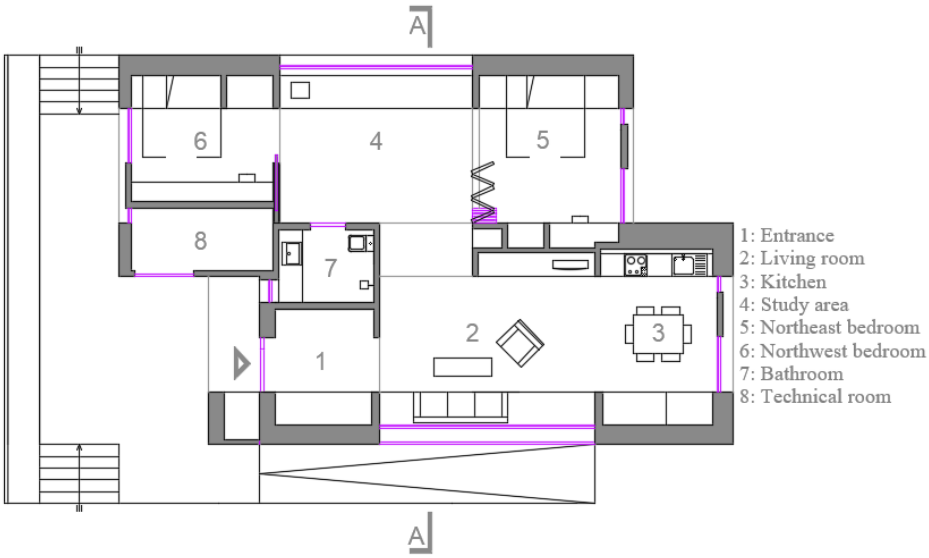

Figure 5.2: Living Lab AutoCAD blueprint with explanations

Table 5.1: Building envelope specifications, Living Lab

Component	Value	Description
Floor	U = 0.1 W/m^2K	Raised timber framed construction, mineral wool insulation, parquet timber flooring
Outer wall	U = 0.11 W/m^2K	Timber framed construction, mineral wool insulation, timber cladding
South window	U = 0.65-0.69 W/m^2K	Triple glazed unit with insulated aluminium frame, double skin
North window	U = 0.97 W/m^2K	Triple glazed unit with insulated aluminium frame, double skin
East and west doors	U = 0.8 W/m^2K	Aluminium clad timber framed triple glazed units, integrated vacuum insulated panels
Roof	U = 0.1 W/m^2K	Timber framed construction, mineral wool insulation, integrated phase change material, in-roof photovoltaic panels
Roof lights	U = 1.0 W/m^2K	Aluminium clad timber frame, triple glazed
Normalized thermal bridge	$\Psi = 0.03$ W/m^2K	Detailed thermal bridge design
Air tightness	0.3 ACH at 50Pa	Detailed design of a continuous vapor and wind barrier, pressure tested

Table 5.2: External wall layers, Living Lab

#	Material	Thickness [m]
1	Cladding (Alvdal)	0.022
2	Airgap	0.044
3	UV Proof barrier	-
4	Rockwool	0.2
5	Vapor barrier	-
6	Rockwool	0.15
7	Wooden battons	15%
8	Vapor barrier	-
9	Airgap	0.048
10	Plywood panels	0.015
Total		0.479

Technical installations

The heating system is comprised of a 3.2 kW ground-source heat pump with a coefficient of performance (COP) of 3.69, when the thermal output is for heating (35 ° C). When the heat pump operates at a higher thermal load for domestic hot water use (55 ° C) the nominal output is 2.6 kW with a COP of 3.0 (Wiik, 2017). The heat pump is connected to a horizontal surface collector field, located at the north side of the building. The total pipe length is approximately 130 m. The heat pump is coupled with a hot water storage tank and two thermal collectors. The heat pump compressor is a fixed speed scroll compressor, with the working fluid R134a. The floors have hydronic heating, in addition there is a radiator connected to the thermal storage tank. The radiator is placed in the living room of the building. Living Lab is not equipped with a mechanical cooling system, but takes advantage of passive cooling strategies. The balanced mechanical ventilation system has a nominal air flow rate of 120 m^3/h, with a total capacity of 360 m^3/h (Goia et al., 2015). A rotating heat exchanger is placed in the central air handling unit, with an efficiency of 0.85 in flow-rate conditions of 250 m^3/h. There is also an electric heating coil in the air handling unit with a capacity of 1200 W, that is able to preheat the air to 40 ° C for ventilating heating purposes. The air diffusers are placed in the bedrooms, living room and study area. The air extracts are placed in the kitchen and the bathroom. Details regarding the technical installations in Living Lab will be further elaborated upon in section 6.3.2 to avoid repetition of information.

Figure 5.3: Inside the technical room in Living Lab

Chapter 6

Methodology

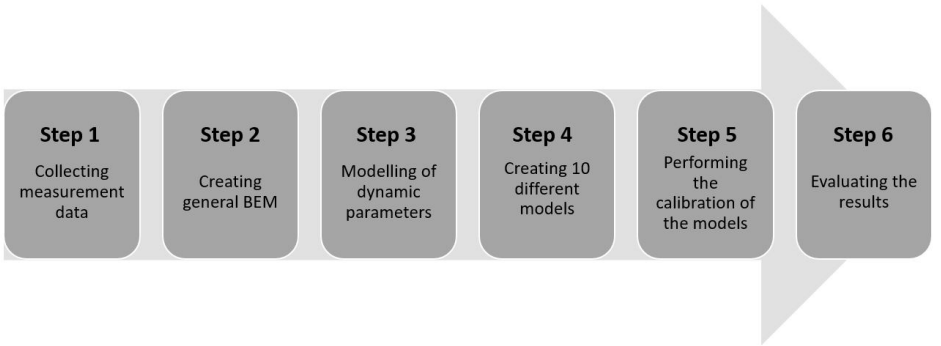

Figure 6.1: Methodology process

The steps followed to investigate the optimization-based calibration of Living Lab parameters are illustrated in figure 6.1. Step 1 in the process was to collect measurement data. Step 2 involved creating a general EnergyPlus-compatible building energy model (BEM) of Living Lab through the use of the third-party software DesignBuilder V5. The EnergyPlus-file was further modified with the EnergyPlus IDF-Editor. Step 3 was the implementation of different strategies for dynamic parameter modelling. The measurements contained data sets of hourly internal gains in the living room, as well as the heating power and supply/return temperatures from the water radiator and supply air temperatures from the air handling unit. These measurements were used in step 3 for dynamic parameter scheduling. Step 4 was the creation of the 10 different energy models of Living Lab with varying degrees of dynamic parameter scheduling from measurement data. Step 5 included the actual calibration of the models with the optimization-based multi-objective calibration algorithm in Matlab. Finally, the results were evaluated in step 6.

6.1 Step 1: Collecting measurement data

The first step in the process was to collect measurement data from Living Lab. This is a very important first step in the calibration of building parameters, especially considering buildings with advanced HVAC systems. The building energy model may be adjusted and simplified if there is information about parts of the heating, ventilation or cooling systems that are turned off during the measurement period. Simplifying the model may potentially yield considerable time savings.

The measurement data was obtained through the PhD-student and co-advisor of this master thesis, Kristian Skeie. The fact that the Living Lab is a research facility complicated the process of finding a data set fit for purpose. Measurement data from Living Lab is abundant, but ideally it should be from a regular-use period where both occupancy and heating settings are well documented. In the data sets that were originally intended for the calibration, it was found that the heating system was controlled by a pre-computed pseudo random binary sequence (PRBS) (Vogler-Finck et al., 2017). Although the measurement data contained the hourly heating power, it was hard to replicate the HVAC setting in a building energy model, not enabling a comparison between the modelling strategies. To minimize the potential calibration errors, the heating control operation should be simple and leave out as many potential modelling errors as possible. Another data set was needed with a set point temperature as the heating control.

One of the obtained data sets were measurements registered from the period of 13.12.2018 - 10.01.2019. In this period, Living Lab was unoccupied. The hydronic floor heating was turned off, leaving the water radiator in the living room and the heating coils in the air handling unit as the main heating sources. The set point temperature for heating was $22°C$. This data set was chosen for further calibration purposes. The calibration algorithm was originally intended for ANSI/ASHRAE Standard 140-2001 (BESTEST), Case 600 (Henninger and Witte, 2004). This is a low mass imaginary building with only one thermal zone. It was found that the best manner to implement the algorithm on a real building with several zones was to adjust the calibration to one specific zone. It was decided to focus on the main area of Living Lab, which was modelled to be a compilation of the kitchen, the living room and the study area. The indoor air temperature in this zone was measured by several sensors. Five sensors were placed at the north wall in different heights, to investigate air temperature stratification. The same measurement configuration existed for the south wall. There was also one sensor placed in the kitchen. In EnergyPlus, the air temperature for each zone is averaged. For this reason, the measured temperature for the main area was obtained by calculating the average temperature given by the eleven sensors. It was chosen to calibrate the building based on the measurements done in week 51 and week 52, 2018. This period had seemingly stable measurements without abrupt peaks in temperature or heating power. Such peaks may be caused by errors originating from the measurement devices and should hence be avoided in calibration data sets. The averaged indoor air temperatures for the calibration period were chosen as the key performance indicator and is shown in figure 6.2.

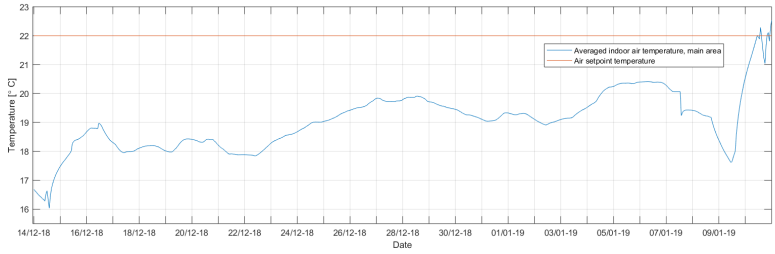

Figure 6.2: Indoor temperature measurements from Living Lab - 13.12.2018-10.01.2019

Table 6.1: Volume and area for Living Lab BEM zones

Zone	**Area** $[m^2]$	**Conditioned**	**Volume** $[m^3]$
Northwest bedroom	12.90	Yes	46.11
Northeast bedroom	16.80	Yes	57.35
Technical room	6.25	No	18.11
Main area	69.12	Yes	235.76
Bathroom	4.87	Yes	16.78
Total	**103.68**		**356.00**
Conditioned total	*103.68*		*356.00*
Unconditioned total	*6.25*		*18.11*

6.2 Step 2: Building Energy Model (BEM)

This section deals with the modelling of Living Lab that is kept similar for all of the ten models. The internal gains and HVAC settings are treated in separate chapters.

6.2.1 Geometry and zoning

The geometry of Living Lab was found on the basis of AutoCAD .dwg files. Each height was carefully measured to obtain as correct volume as possible. Figure 6.3 shows the final geometrical result. The zoning is shown in figure 6.4. This configuration was chosen on the basis of internal partitions rather than differences in solar irradiation. Hence, the indoor air temperature in the zone ”Main area” will resemble the averaged temperature obtained from the previously described measurement data. Furthermore, the building was unoccupied during the measurement period, leaving out the need for different occupancy pattern schedules for the zones. The zone ”Technical room” is included in the thermal calculations, however it is modelled with the template ”No heating or cooling”. Due to the placement of heat-emitting technical installations inside the room, it was considered to include internal heat gains in the zone to imitate the conduction heat transfer through the inner partitions facing the zone. Simulation runs with both alternatives were tried, revealing a negligible difference. It was for this reason decided to turn the internal gains off. The final volume and area of the modelled zones are presented in table 6.1.

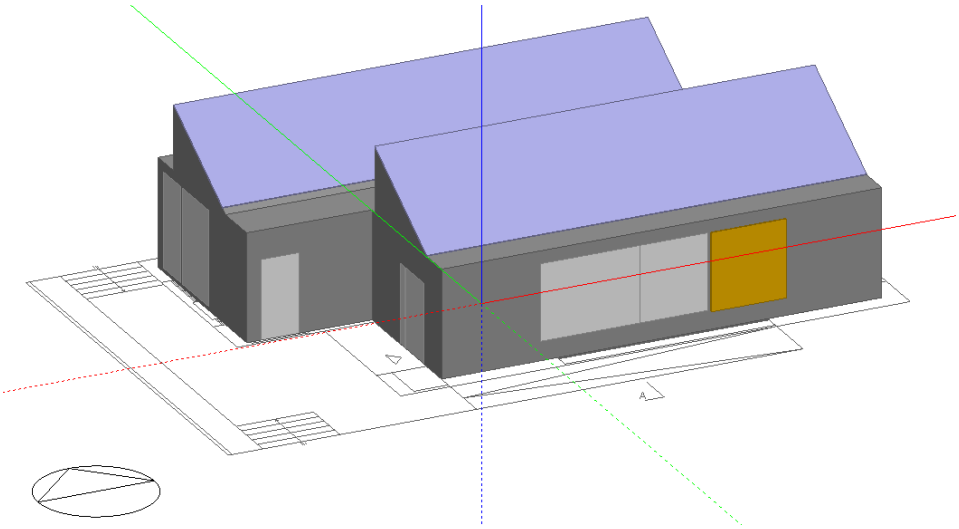

Figure 6.3: Living Lab BEM created with DesignBuilder

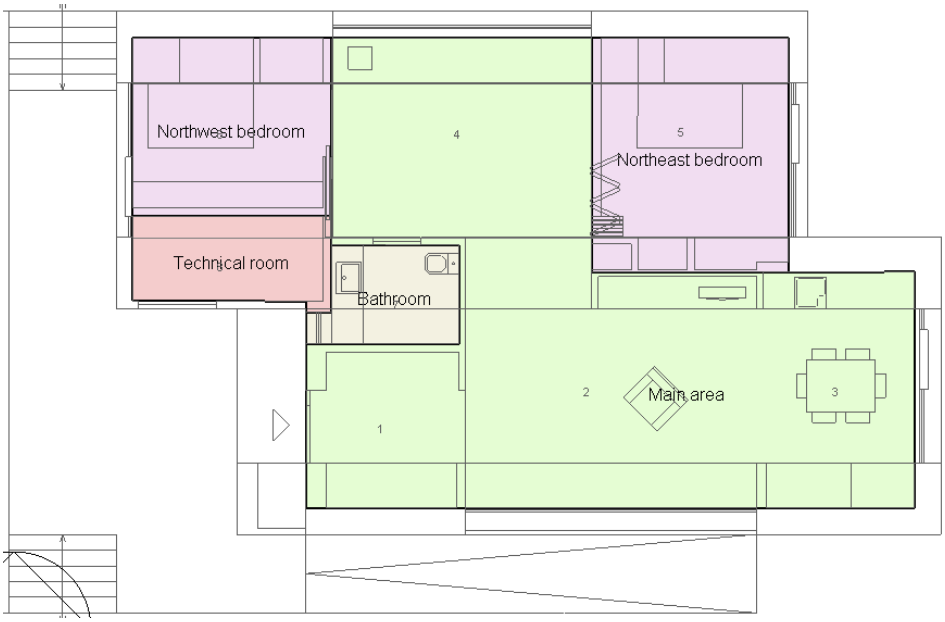

Figure 6.4: Chosen zone partitions of Living Lab

Table 6.2: Material layers used in Living Lab model

Layer	External wall	Floor	Tilted roof	Flat roof	External door
1	Cladding *0.022 m*	Hardboard *0.250 m*	Roofing *0.002 m*	Roofing *0.002 m*	Cladding *0.022 m*
2	Airgap *0.044 m*	Chipboard *0.022 m*	Rockwool *0.400 m*	Rockwool *0.260 m*	Rockwool *0.250 m*
3	Rockwool *0.350 m*	Rockwool *0.400 m*	Airgap *0.048 m*	Polystyrene *0.020 m*	Plywood *0.020 m*
4	Airgap *0.048 m*	Plywood *0.022 m*	Concrete *0.005 m*	Gypsum *0.015 m*	
5	Plywood *0.015 m*		Plywood *0.015 m*	Rockwool *0.1 m*	
6				Airgap *0.048 m*	
7				Plywood *0.015 m*	

6.2.2 Construction

Walls, roof, floor and doors

Table 6.2 presents the material layers in the construction. They were chosen on the basis of the presentation of Living Lab by Carlucci (2019). Density, specific heat and thermal conductivity for the materials were inserted based on tabulated values for materials found in table 21 and 22 in *ByggForsk 410.010 – Varmekonduktivitet og varmemotstand for bygningsmaterialer*. Byggforsk is a *SINTEF*-developed series with documented solutions and recommendations for the engineering, execution and management of buildings (SINTEF Byggforsk, 2019). Regarding the heat transfer, the insulation thickness is the main contributor for the total U-value of the construction. This is due to the considerably lower thermal conductivity in the insulation material compared to the other materials. Some layers, like the vapor and wind layers, did not affect the construction U-value, for this reason they were neglected. The vapor and wind layers are important parameters in terms of the infiltration rate, but the infiltration is modelled in the software on the basis of the inserted airtightness of the building. The infiltration rate was defined as constant $0.3\ AC/h$ at a pressure difference of $50\ Pa$, as given in the presented information.

The internal sliding doors that separate the main area with the bedrooms were modelled as openings. This was a simplification compared to modelling internal doors that were always open. However, the bathroom door was modelled as an internal door. This was due to the uncertainty in terms of the door position during the measurement period. The majority of the air is extracted through the bathroom vent. To ensure the balanced air flow, the final decision was to schedule the door as always open.

Table 6.3: Window specifications, Living Lab model

	South window	**North window**
U-value	0.69	0.98
Total solar transmission	0.199	0.474
Direct solar transmission	0.162	0.358
Light transmission	0.346	0.661
Number of layers	3	3
Window gas type	Argon	Argon

PCM layer in tilted roof

There is a layer of a phase-changing material (PCM) in the tilted roof. Such materials have the possibility of melting and solidifying at certain temperatures, enabling them to store thermal energy. The energy is released when the material undergoes transitions in state. Adding PCM layers in buildings is a means of increasing the thermal mass and hereby reduce fluctuations in air temperature. The panels are of the type Dupont Energain (2010) which melts at 22°C and solidifies at 18°C. The real effect of the PCM layers in Living Lab is unknown, especially due to the fact that there is a plywood layer covering the material (Kristian Skeie, personal interview, April 2019). There is a means of implementing PCM layers in EnergyPlus, however it requires detailed transient modelling. This solution is not desirable with an optimization-based calibration that will run the simulations 980 times for each model. Hence, it was decided to add a $0.02\ m$ layer of concrete for the tilted roof section to account for the PCM layer. The concrete layer yielded a slight reduction in indoor air temperature fluctuations during the simulation testing.

Windows and window shading

In the investigated zone, there are windows facing both north and south. The specifications of the modelled windows are tabulated in table 6.3. It should be noted that the south window have a 30 cm air gap between the triple-paned inner window and the outermost pane. This gap is designed for ventilative purposes. It was decided not to include this air gap in the model, as it was informed that the ventilation was not active during the measurement period. For the windows facing east and west, the total U-value were not found in the information, but the panes share similarities with the southern windows. For that reason, it was considered a reasonable estimation to use the south window template.

The north windows do not have any kind of shading. For the south facing windows, there is a possibility of inside shading with manual control, as seen in picture 6.5. The state of the shading during the measurement period is unknown. The measurements are taken from a cold winter period with minimum solar irradiation. In addition, when the shading devices are placed inside the building, the effect on solar heat gain is low compared to using outside shading. However, it was decided to do simulations to test the potential differences in terms of the indoor air temperature. Figure 6.6 shows that the results are negligible. It important to note that the effect would be greater if the building was calibrated with measurement data taken from a summer period.

Figure 6.5: South facing windows with solar thermal collector, Living Lab

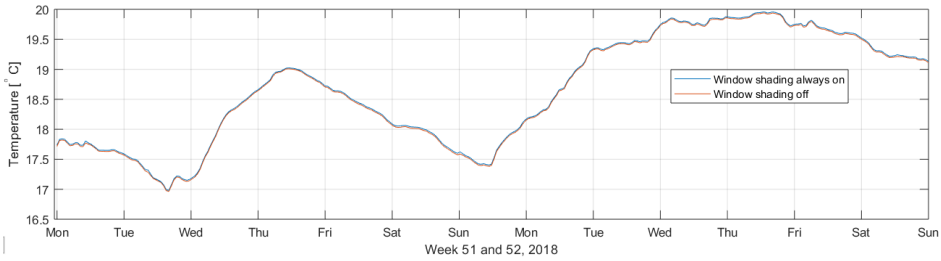

Figure 6.6: Main area zone temperature with south window shading always on/off

Thermal bridges

In the Living Lab documentation, a normalized thermal bridge value of $\psi = 0.03\,W/mK$ was given. In EnergyPlus, there are two options when it comes to inserting thermal bridge values. The first option is to exclude the calculation of thermal bridges, whereas the other option is to insert specific values for each thermal bridge component. As there is no manner of differentiating the normalized value into the individual components without more detailed information, the latter alternative was chosen. It was done a brief literature review to investigate the typical values for thermal bridges in passive houses. In an article by Rohdin et al. (2014), nine Swedish passive houses were investigated. Table 6.4 shows the values. Based on this information, the estimated thermal bridge values for Living Lab inserted in the EnergyPlus model are shown in table 6.5.

Table 6.4: Thermal bridge values from nine Swedish passive houses

Thermal bridges $[W/mK]$	**Value**
Edge beam	0.094
Corner wall	0.027
Windows and doors	0.041
Wall/joist	0.025

Table 6.5: Thermal bridge values inserted in EnergyPlus

Thermal bridges [W/mK]	**Value**
Roof-Wall	0.094
Wall-Ground floor	0.094
Wall-wall	0.027
Wall-floor	0.094
Lintel above window or door	0.041
Sill below window	0.041
Jamb at window or door	0.041

Ground

Living Lab does not reside on a concrete foundation, but wooden batons with a $10\ cm$ air gap between the ground and the outermost floor layer. This was taken into account in the modelling by defining the outermost layer as air. The ground temperature is of importance due to both the thermal heat loss, but specifically in this model due to the ground source heat pump configuration. As will be elaborated upon in the chapter 6.3.2, the ground heat exchanger operates with the set point manager *follow ground temperature*. The reference ground temperature type is chosen as shallow, as the configuration is horizontal. According to de Beer (2017), the ground temperature is on average 1-2 °C higher than the average annual air temperature at the site. However, this is the deep ground temperature. The shallow ground temperature may be lower in the winter season. The averaged annual temperature for Trondheim in 2018 was found to be 6.7 °C, by accessing the weather database *eKlima*. Simulations with shallow ground temperatures ranging from $0 - 8.7\ ^{\circ}C$ were done in DesignBuilder. The difference in temperatures did not affect the results, meaning the heat pump had sufficient capacity to supply the radiator even with lower ground temperatures. In the final model, the shallow ground temperature was set to $1\ ^{\circ}C$.

Photovoltaic panels and thermal solar collector

There are two photovoltaic panels located on the roof, occupying a total of approximately $80\ m^2$. The panels are an important contributor to the ZEB definition of Living Lab. However, the aim of the thesis does not include the primary energy usage or greenhouse gas emission calculations. In addition, the calibration will be performed for two weeks in a winter period. The inclusion of the panels will increase simulation time, but not contribute with relevant data for the calibration. The same arguments are also applicable for the decision to exclude the thermal solar collectors in the model. The PV panels and the thermal solar collector are represented in figure 6.3 for visual purposes, however they are not included in the EnergyPlus model.

External shading

The location of Living Lab can be described as semi-exposed in terms of shading. One tall building, *Verkstedtekniske Laboratorier*, is facing the west facade. This building is

approximately 15 m tall, situated approximately 25 m from Living Lab. The shading does affect the photo-voltaic electricity production and the solar irradiation gains on the west facade. However, only a fraction of the west facade is represented in the main area zone, as seen in figure 6.4. In addition, the heating and cooling contributions from solar irradiation may be considered as minimal in the winter period, shown in figure 6.9 in the following weather data section. The effect of window shading was tested and found negligible for the southern windows in section 6.2.2. The effect of shading from external objects is dynamically calculated in EnergyPlus as a function of solar position and may contribute to considerable additional computation time. As the PV panels are not included, in addition to the orientation towards west, it was decided to exclude the shading in the model.

6.2.3 Weather data

When calibrating a building energy model, the weather file is of great importance. The temperature is an essential variable when it comes to heating and cooling demand, together with the solar irradiation on the building surface. The pressure difference between the interior of the building and the exterior is dependant on the wind speed, which plays an important role in terms of infiltration. Trondheim is not included in the weather file library for EnergyPlus. A weather file for 2018 was needed to enable the calibration. The Norwegian Meterological Institute offers a service called $eKlima$, a large free access climate database with measurements from various weather stations in Norway (Norwegian Meteorological Institute, 2019). The nearest weather station was found to be in Voll, Trondheim. The distance between the locations is approximately 2.26 kilometers. Regarding altitude, Living Lab is located 54,5 meters above sea level whilst Voll weather station is located 127 meters above sea level.

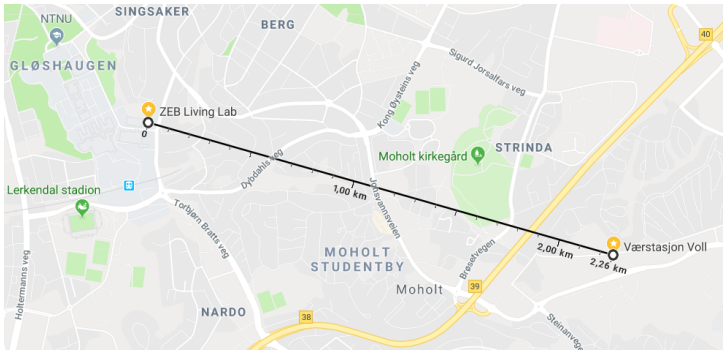

Figure 6.7: Distance from Living Lab to Voll weather station (Google Maps, 2019)

The ideal weather file would be based on measurements from Living Lab. The obtained measurement data was not sufficient to achieve a coherent weather file. There were no measurements regarding wind speed or relative humidity. Subsequently, it was decided that the relative humidity and wind speed data from Voll were used further.

It was a total of four different measurements regarding the outdoor dry-bulb temperature. The first option was measurements that were taken every hour. The second option was

averaged hourly measurements, where the temperature sensor had recorded several measurements each hour. The third option was to use hourly temperature data from sensors located on the north and south wall. These north and south temperatures were averaged and plotted against the other measurements. In figure 6.8, the averaged measured indoor temperature in the main area is also plotted. It can be seen that the relationship between the indoor and outdoor temperature is more apparent for the second week. For the weather file, the averaged hourly temperatures from the north and south wall were used further due to similarity in the slope compared to the measured indoor temperatures. The measurements from the two week calibration period were merged with the temperatures from Voll for the remaining year.

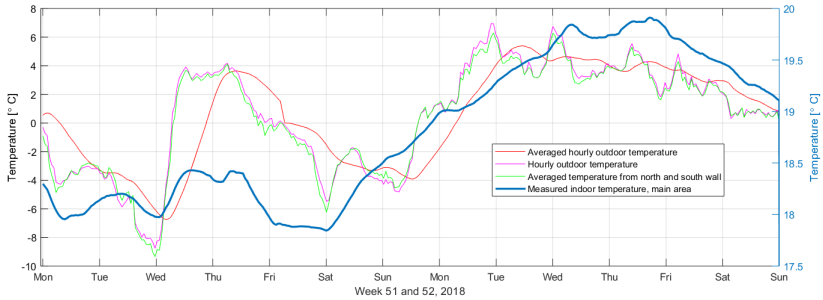

Figure 6.8: Outdoor temperature measurements from Living Lab

An important weather variable that was neither included in the statistics from Voll, nor Living Lab, was the solar irradiation. This information was provided by the European Union's service Copernicus (European Union, 2019). After collecting all of the desired variables, an EnergyPlus-compatible *.epw* weather file was created by the use of the software Elements, provided by Big Ladder Software (Big Ladder Software, 2019). Figure 6.9 and 6.10 show the obtained hourly solar irradiation and dry-bulb air temperature measurements for 2018.

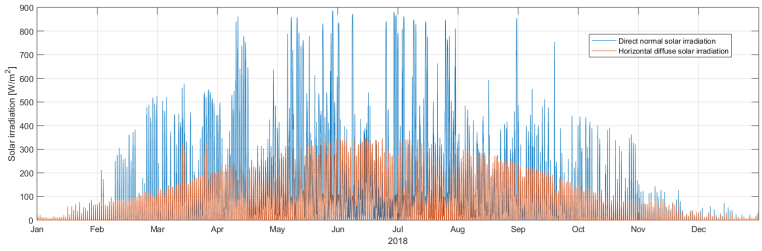

Figure 6.9: Solar irradiation for 2018, Voll weather station

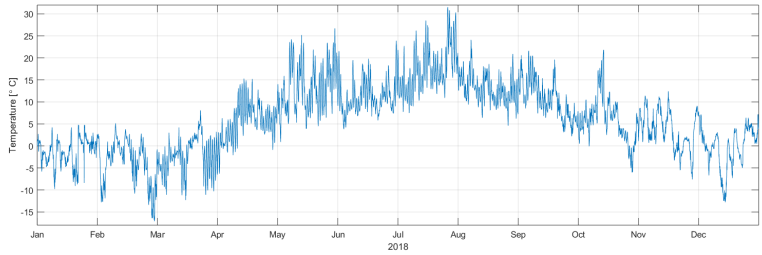

Figure 6.10: Air temperature for 2018, merged measurements from Voll and Living Lab

6.3 Step 3: Modelling of dynamic parameters

After the general building energy model was created, different strategies were investigated for the modelling of dynamic parameters. Below is a list which describes the different approaches.

- Internal gains
    1. *Not scheduled*: The internal gains during the measurement period were averaged and inserted as a constant value
    2. *Scheduled*: The hourly variation in internal gains was implemented with a schedule
- Radiator heating power
    1. *Not scheduled*: A coherent HVAC model was created with the correct set points and design capacities according to available information
    2. *Scheduled power*: The water radiator was removed from the model and replaced as internal gain. The hourly variation in radiator power was implemented with a schedule
    3. *Scheduled supply temperature*: The supply temperature for the water radiator was taken from measurements and implemented as a schedule in a set point manager
- Air handling unit supply temperature
    1. *Not scheduled*: The given set point temperature of 19°C was used for the air temperature leaving the air handling unit
    2. *Scheduled*: The hourly temperatures taken from measurements were implemented with the use of a schedule in a set point manager

6.3.1 Internal gains

It was found a power consumption from two of the power sockets in the living room, in addition to the power consumption from the fridge. Figure 6.11 shows the power inserted in

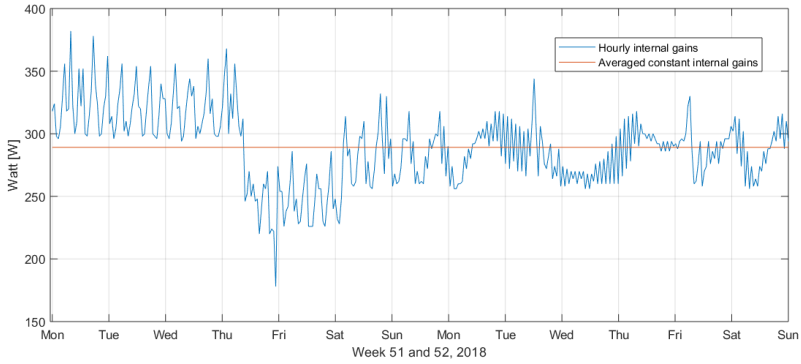

Figure 6.11: Measured internal gains in zone

the model for the two solutions. The average power consumption was $289.13\ W$, whereas the hourly consumption fluctuated between $67.2 - 382\ W$. Table 6.6 shows the different settings chosen. The internal gains were inserted under the tab "Other equipment". The schedule *InternalGains* was created by making a schedule file, visualized in figure 6.12. The $.txt$-file was a 8760x1 matrix with hourly fractions of the maximum internal gain power.

```
Schedule:File,
    InternalGains,           !- Name
    Fraction,                !- Schedule Type Limits Name
    C:\Users\karolibh\Documents\MATLAB Karoline\IntGaintxt.txt,  !- File Name
    1,                       !- Column Number
    0,                       !- Rows to Skip at Top
    8760,                    !- Number of Hours of Data
    Comma,                   !- Column Separator
    No;                      !- Interpolate to Timestep
```

Figure 6.12: Schedule for internal gains

6.3.2 HVAC system

This subchapter elaborates on the different configurations chosen for the HVAC modelling. A detailed HVAC system was needed to enable analysis of calibration models where the water radiator heating power was not treated as scheduled internal gains. In addition, the air handling unit is included in all of the models.

Heat pump

The HVAC system in Living Lab was modelled as seen in figure 6.13. The heat pump is connected to horizontal boreholes, with a rated heating capacity of $11070\ W$ and a rated electricity consumption of $3000\ W$. The thermal storage tank is not included in the model. The domestic hot water use was set to zero in all of the models due to the lack of occupancy

Table 6.6: Different strategies for implementing internal gains

Field	**Units**	***Not scheduled***	***Scheduled***
Name		Block7:MainArea Equipment 1	Block7:MainArea Equipment 1
Fuel Type		Electricity	Electricity
Zone or ZoneList Name		Block7:MainArea	Block7:MainArea
Schedule Name		On	InternalGains
Design Level Calculation Method		Watts/Area	Watts/Area
Power per Zone Floor Area	W/m2	4.183063272	5.52662037
Fraction Radiant		0.5	0.5

during the measurement period. The storage tank is also connected to the heat pump and the solar thermal collectors. As described in chapter 6.2.2, the solar thermal collectors are not included in the building energy models. As long as the heat pump is able to deliver the desired water temperature to the radiator and the water heating coil in the air handling unit, the configuration previous to the water entering the radiator and the heating coil is of less significance in the building energy model. The chosen key performance indicator is the indoor air temperature. If the calibration algorithm was run with energy use as the key performance indicator, it would have been important to include the thermal storage tank. The set point temperature for the water leaving the heat pump was chosen to be $35^{\circ}\ C$, because this was the set point temperature stated for heating (Wiik, 2017).

Water radiator

Option 1: Modelling the radiator

The water radiator in the model is connected to a zone group. This group consist of the bedrooms, the main area and the bathroom. However, the radiators are scheduled as "Off 24/7" for every zone with exception of the main area. The water radiator configurations are taken from the producer catalogue (Lyngson, 2005). The heating design capacity was found by looking at an Excel-file with results from experiments conducted in LivingLab, provided by co-advisor Kristian Skeie. The maximum water flow rate was chosen based on the maximum flow rate from the measurement data. Table 6.7 shows the chosen settings.

Option 2: Modelling the radiator as internal gains

The other method chosen for implementing the heating power from the water radiator, was to model it as internal gains with an hourly heating power schedule derived from measurement data. Figure 6.14 shows the power fluctuations during the measured period.

The schedule is presented in figure 6.15. The $.txt$-file was, similarly to in the internal gain case, a 8760x1 matrix with fractions of the maximum power emitted, being 4620 W.

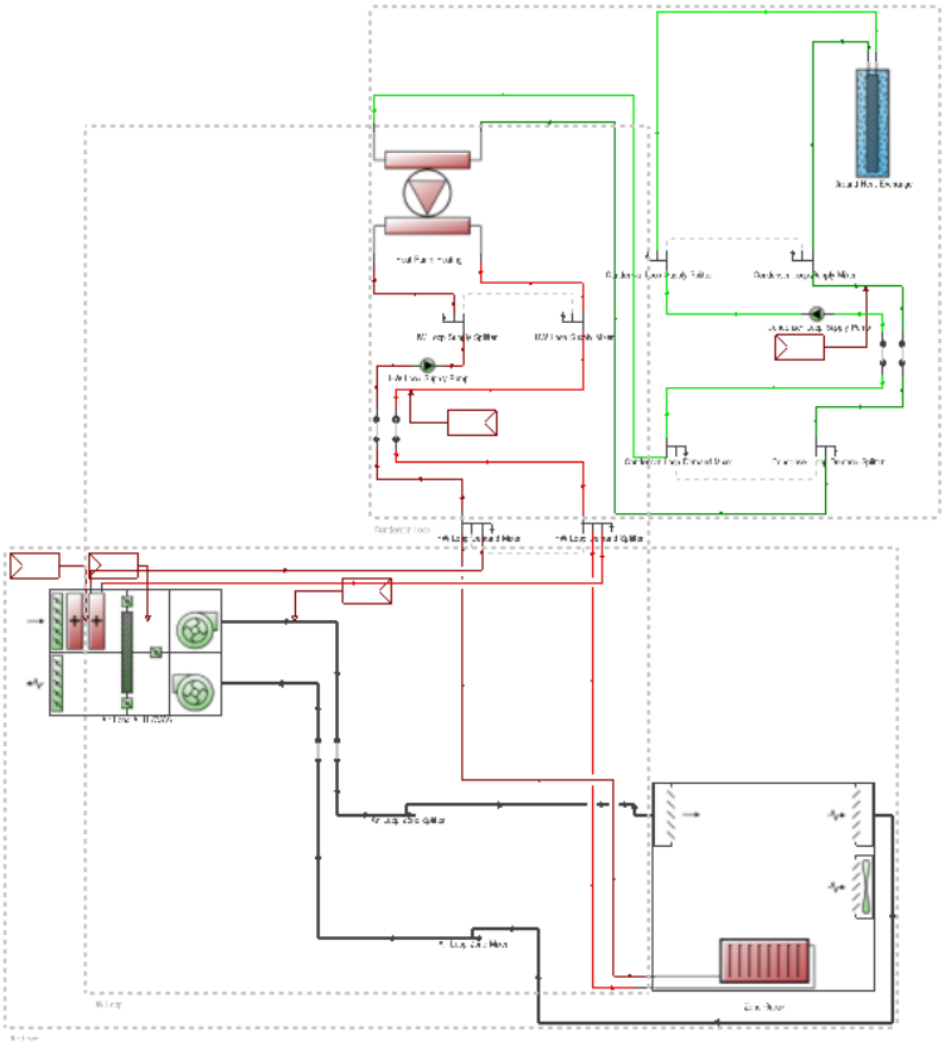

Figure 6.13: Detailed HVAC plant model

Option 3: Scheduling the supply temperature for the water radiator

As opposed to modelling the actual power rate as internal gains, it was tested to keep the radiator configuration and rather insert a set point manager between the heat pump and the water radiator with a temperature schedule consisting of the actual measured supply temperature for the water radiator. This ensured that the water radiator temperature in the model and in reality was kept similar. The temperatures are seen in figure 6.15.

Table 6.7: Water radiator settings in BEM

Variable	Value
Heating design capacity $[W]$	4620
Maximum water flow rate $[m^3/s]$	0.000031
Rated average water temperature $[°C]$	70
Rated water mass flow rate $[kg/s]$	0.0630
Fraction radiant	0.3
Fraction of radiant energy incident in people	0.1
Schedule	On 24/7

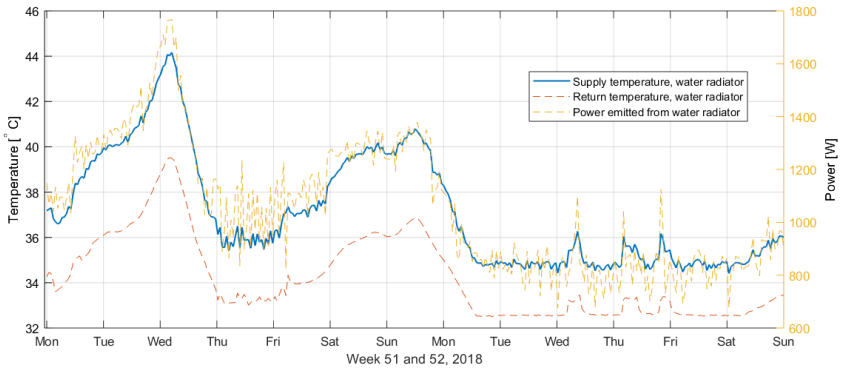

Figure 6.14: Radiator power, supply and return temperature in the measured period

```
Schedule:File,
    RadIntGain,               !- Name
    Fraction,                 !- Schedule Type Limits Name
    C:\Users\karolibh\Documents\MATLAB Karoline\RadIntGaintxt.txt,  !- File Name
    1,                        !- Column Number
    0,                        !- Rows to Skip at Top
    8760,                     !- Number of Hours of Data
    Comma,                    !- Column Separator
    No;                       !- Interpolate to Timestep
```

Figure 6.15: Schedule for water radiator

6.3.3 Air handling unit

A balanced mechanical CAV ventilation system with heat recovery and two heating coils was inserted in the model. Table 6.8 shows the configuration for the air handling unit, based on information by Goia et al. (2015). The air inlets and exhaust vents were placed as described in chapter 5.1.1. A total nominal air flow of 144 m^3/h was used. The air extract and supply to the different zones seen in table 6.9 are based on values from the master thesis titled *Moisture Production in Buildings* written by Pedersen (2018). Co-supervisor Kristian Skeie informed that the settings had not been changed to date. The supply temperature leaving the AHU were modelled in two different ways.

Table 6.8: Air handling unit settings in BEM

Variable	Value
Nominal capacity, electrical heating coil	1200 W
Heating design capacity, water heating coil	2000 W
Nominal supply air flow rate, AHU	0.04 m^3/s
Heat exchanger type, AHU	Rotary
Effectiveness heat exchanger, AHU	0.85
Fan total efficiency, supply and extract fan	0.7
Pressure rise, supply and extract fan	600 Pa

Table 6.9: AHU air supply to zones in BEM

Zone	Air supplied	Air extracted
Northwest bedroom	26 m^3/h	0 m^3/h
Northeast bedroom	52 m^3/h	0 m^3/h
Bathroom	0 m^3/h	108 m^3/h
Main area	66 m^3/h	36 m^3/h
Total	144 m^3/h	144 m^3/h

Option 1: Constant set point temperature

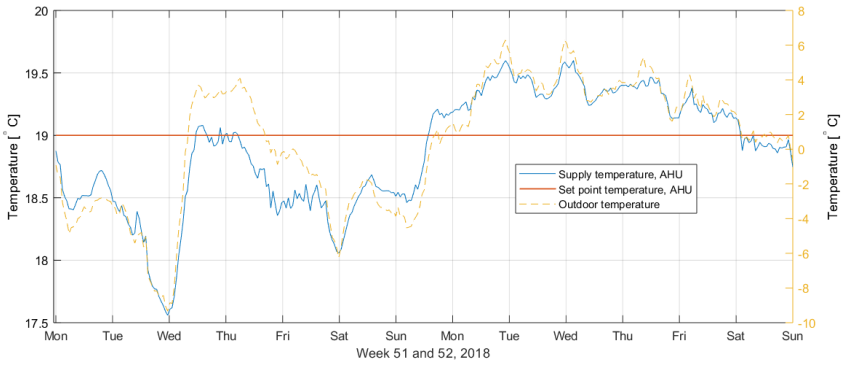

Figure 6.16: Air handling unit supply temperatures

The first option was to insert the given set point temperature of 19 °C in the set point manager for air leaving the air handling unit.

Option 2: Scheduled set point temperature

As figure 6.16 shows, actual supply temperature was fluctuating around the set point. The fluctuation is related to the outdoor temperature. The second modelling option consisted of inserting a temperature schedule for the set point manager for air leaving the AHU.

The *.txt*-file was this time a 8760x1 matrix with actual supply temperatures from the calibration period taken from the measurement data.

```
Schedule:File,
    AHUsetpoint,            !- Name
    Temperature,            !- Schedule Type Limits Name
    C:\Users\karolibh\Documents\MATLAB Karoline\scheduleAHUtxt.txt,  !- File Name
    1,                      !- Column Number
    0,                      !- Rows to Skip at Top
    8760,                   !- Number of Hours of Data
    Comma,                  !- Column Separator
    No;                     !- Interpolate to Timestep
```

Figure 6.17: Schedule for AHU supply air

6.4 Step 4: Creating the 10 energy models

Table 6.10 shows the 10 different building energy models that were created. The value ”Yes” signifies that hourly measurement data is used, whereas the value ”No” means that no measurement data were used. The radiator supply temperature and the heating power implemented as internal gains were not simultaneously scheduled, as they were conflicting. The explanation of the models will be further elaborated in chapter 7.

Table 6.10: Calibration models

	Internal gains	**Radiator supply temperature**	**Radiator heating power**	**AHU supply temperature**
Model 0	*No*	*No*	*No*	*No*
Model 1	*Yes*	*No*	*No*	*No*
Model 2	*No*	*Yes*	*No*	*No*
Model 3	*No*	*No*	*Yes*	*No*
Model 4	*No*	*No*	*No*	*Yes*
Model 5	*Yes*	*Yes*	*No*	*No*
Model 6	*No*	*No*	*Yes*	*Yes*
Model 7	*Yes*	*No*	*No*	*Yes*
Model 8	*Yes*	*Yes*	*No*	*Yes*
Model 9	*Yes*	*No*	*Yes*	*Yes*

6.5 Step 5: Performing the optimization-based calibration

After finishing the building energy models of Living Lab, the models were implemented into the optimization-based calibration algorithm. The algorithm was originally tested for the simulation software EnergyPlus with the test building ASHRAE BESTEST Case 600. The move from a simplistic, single-zone construction with ideal heating and cooling, to a

complex building like Living Lab, offered some challenges with regards to adjustments in the algorithm and demanded a clear view in terms of the modelling of the building. Figure 6.18 shows the options when it comes to choosing the time period, the key performance indicator (KPI) and the error functions in the algorithm.

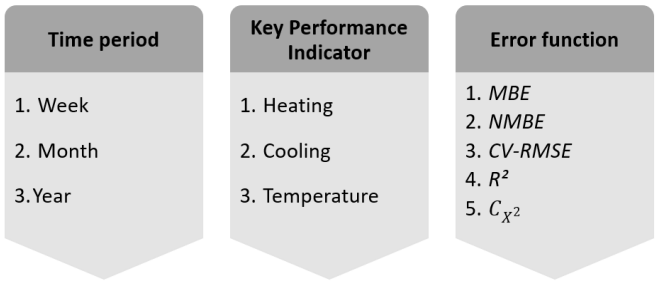

Figure 6.18: Calibration algorithm options

6.5.1 Selection of calibration options

Time period

The algorithm has three options regarding the time period the calibration will be run. This option will be decided based on the obtained measurement data, as it may be difficult to achieve a coherent set of hourly measurement data from a full year of regular building operation. There are both advantages and disadvantages when it comes to the choosing of duration of the calibrated period. Deviations in for instance set point temperatures, occupancy and heating/cooling/ventilation strategies should desirably be thoroughly documented, or measured by the use of sensors. If the obtained data set is taken from a period with discontinued use, or there have been done changes in for instance the HVAC operation, this should be reflected in the building energy model. The calibrated model will lack validity if the conditions in which the building is operated is not reflected in the BEM settings. A short calibration period may on the other hand be insufficient to reflect the fluctuations in temperature that may be caused by the amount of building thermal mass. As stated in chapter 6.1, it was proven to be a challenging task to obtain fit for purpose measurement data from Living Lab. The most appropriate data set was chosen to be two weeks in December 2018 where set point temperatures for the AHU heating, the water radiator and the indoor air temperature were documented in a manner that could be replicated in the building energy model.

Key Performance Indicator

The indoor mean air temperature in the main area was chosen as the key performance indicator. Choosing the heating as the KPI was not an option due to the fact that the heating is one of the dynamic parameters investigated. Neither was cooling an option, as Living Lab does not contain a mechanical cooling system.

Table 6.11: Calibration variables for the optimization algorithm

	Calibration variable	Real value	Lower bound	Upper bound
1	Insulation thickness, floor	*0.40 m*	*0.30 m*	*0.50 m*
2	Insulation thickness, outer walls	*0.35 m*	*0.25 m*	*0.45 m*
3	Insulation thickness, tilted roof	*0.40 m*	*0.30 m*	*0.50 m*
4	Insulation thickness, first layer, flat roof	*0.26 m*	*0.16 m*	*0.36 m*
5	Conductivity, south window outermost pane	1 W/mK	0.5 W/mK	1.5 W/mK
6	Infiltration, main area	*0.3 ac/h*	*0.1 ac/h*	*0.5 ac/h*
7	Air handling unit flow rate, main area	0.01833 m^3/s	0.00833 m^3/s	0.02833 m^3/s

Error functions

The calibration algorithm has implemented five different error functions to enable the comparison of measured and simulated data. Their methods are described in chapter 4. All of the five functions were tested for the calibration. In the results chapter, the results yielded by the different functions will be evaluated separately and compared.

6.5.2 Definition of calibration variables

Living Lab was chosen as the case study due to the access to both thorough construction data and measurement data. The real value of the calibration variables were known. The aim of the calibrations was to compare the calibrated values given by the algorithm with the known values and see which of the modelling options that yielded the most accurate result. An overview of the selected variables together with the chosen upper and lower bounds for calibration is shown in table 6.11. They were chosen based on their implications on the key performance indicator. It was decided to use variables that did not have an impact on the same parameter, like for instance using both insulation conductivity and insulation thickness.

The population size for each generation of the calibration variables was chosen to be 28, four times higher than the number of calibration variables. It is recommended to reach a total of 1000 simulations for each optimization run (Sandra Martinez, personal interview, 2019). Subsequently, the number of generations was chosen to be 35, giving a total of 980 simulation runs with different variable value combinations. The 10 different models were run in parallel on one of the supercomputers at NTNU. Each model calibration took approximately 47 hours to finish.

6.6 Step 6: Evaluation of results

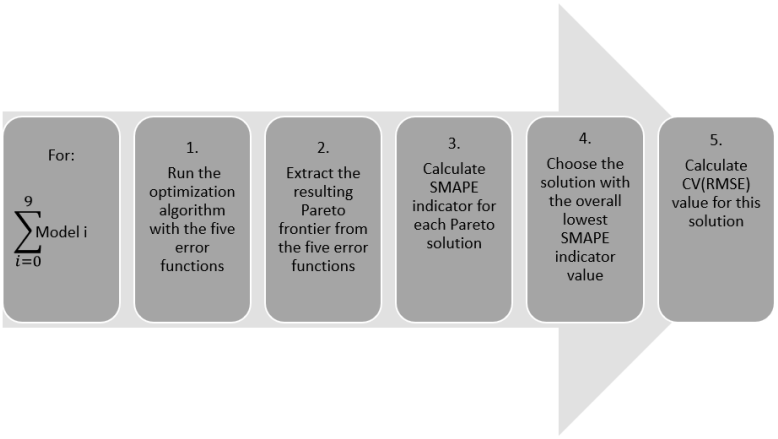

Figure 6.19: Chosen methodology for evaluating the calibration results

To enable the comparison between the calibration outputs given by the 10 different models, the procedure shown in figure 6.19 was followed. Step 1 included the use of the optimization-based calibration algorithm for the 10 models. The procedure for performing step 2, 3, 4 and 5 is shown in the Matlab script 9.2 in the appendix.

Chapter 7

Results and discussion

The results from the optimization-based calibration of the different building energy models will be presented below. The procedure is visualized in figure 6.19. The calibration yielded several optimal solutions for each of the error functions. They are plotted graphically in the form of a Pareto frontier. The Pareto frontiers are located in the appendix, with exception of the Pareto frontier for the base case which is included in the text for visualization purposes. As a means of deciding which Pareto solution that were the closest match to the real calibration variable values, they were evaluated through the use of Symmetric Mean Absolute Percentage Error (SMAPE) indicators. The equation for calculating SMAPE is found in the theory section, whereas the Matlab script for the analysis of the results is located in the appendix. It was found that all of the solutions provided good SMAPE results, consistently below 5%. For this reason, the maximum SMAPE value given by the upper and lower bound of the calibration variables was calculated and found to be 5.418%. This lead to a calculation of the relative value of the SMAPE indicator compared to the maximum possible value, to enable a better visualization of the differences. Nevertheless, the lowest SMAPE values were indeed the optimal solutions yielded by the calibration process. The key performance indicator, being indoor air temperature in this case, was also assessed to investigate the magnitude of compensation effects. For this assessment, the CV(RMSE) score of the key performance indicator was calculated and compared with the situation where the real values of the calibration variables were used in the simulation. A discussion of the results is included below each model section as opposed to in a distinctive discussion chapter, to avoid the repetition of model explanations. An overall discussion of the results is found in the end of the chapter.

7.1 Model 0: Base case

In model 0, none of the dynamic parameters were represented with schedules from measurement data. Internal gains were set constant, and the water radiator power and the AHU supply temperature were given by the configurations in the modelled HVAC system. Figure 7.2 shows the Pareto solutions yielded by the five error functions. It can be seen from

figure 7.1 that the biggest deviation in the results was for calibration variable 6, being the conductivity in the outermost pane of the south window. This variable is not the most sensitive in terms of the results, due to the fact that changing this parameter does not have a big impact on the total south window U-value. The scope of the thesis was to analyze different modelling strategies for dynamic parameters and see how they affected the calibration of a selection of known variables. The magnitude of impact of the variables are not equal. Table 7.1 shows that using the NME error function gave the best solution for model 0 with an optimal SMAPE value of 1.343%.

Table 7.1: Model 0: Best SMAPE indicators

Error function	*NME*	*NMBE*	*CV(RMSE)*	R^2	C_χ
Optimal SMAPE value	**1.343%**	2.238%	1.916%	2.933%	2.309%
Optimal SMAPE value, relative	24.781%	41.304%	35.355%	54.128%	42.623%

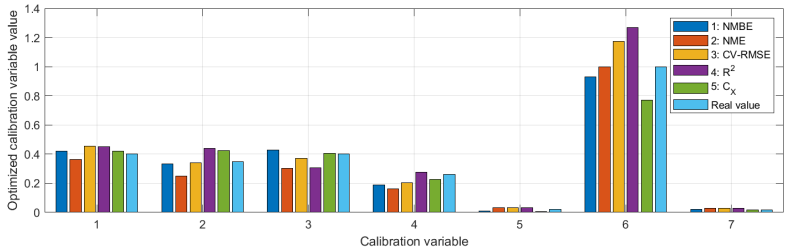

Figure 7.1: Model 0: Optimal values for calibration variables

7.2 Model 1

The only difference between the base case and model 1 is that the internal gains are scheduled with hourly values from measurement data, as opposed to having a constant value. It can be seen in table 7.2 that the overall optimal SMAPE values are lower for this solution, indicating that a dynamic modelling of internal gains were a better solution than a static modelling. Figure 7.4 shows a lower discrepancy between the calibrated values for the error functions, but the insulation thicknesses have a slightly higher value compared to the base case. This may be a compensation effect. The results from the model simulated with known variables yielded higher indoor temperatures than the measured temperatures, as seen in figure 7.3. This caused the calibration process to orient towards values that lowered the indoor air temperature.

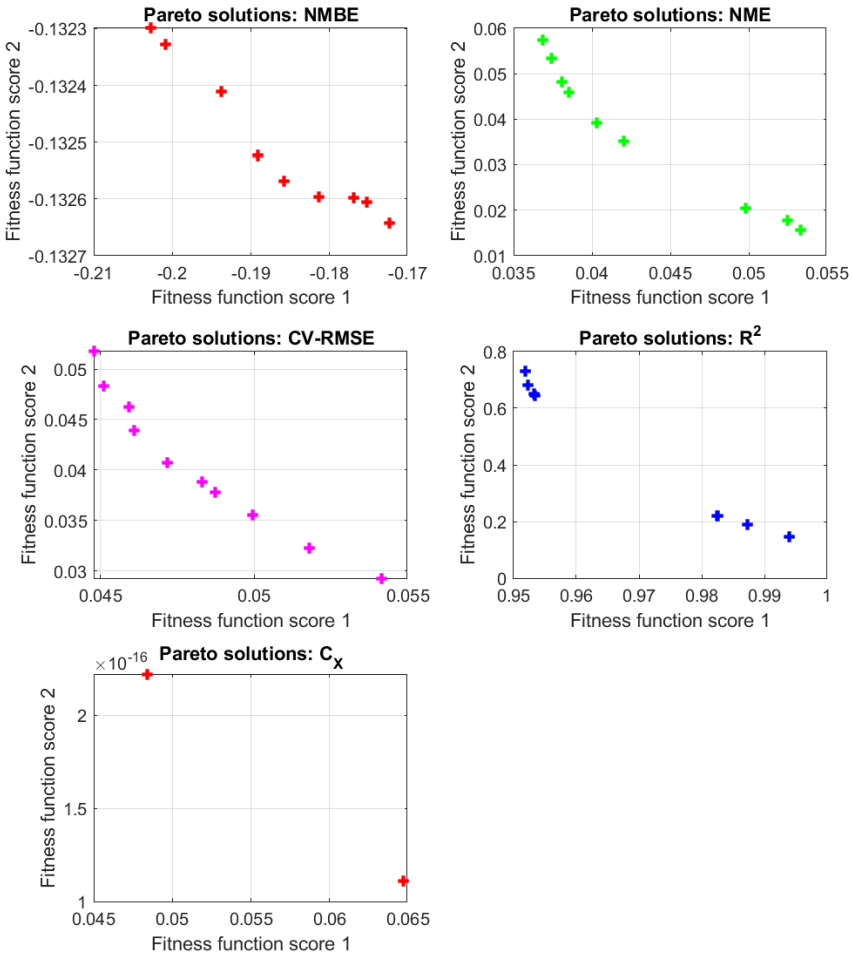

Figure 7.2: Model 0: Pareto solutions

Table 7.2: Model 1: Best SMAPE indicators

Error function	*NME*	*NMBE*	*CV(RMSE)*	R^2	C_χ
Optimal SMAPE value	0.851%	2.004%	**0.721%**	0.937%	1.498%
Optimal SMAPE value, relative	15.709%	36.996%	13.307%	17.295%	27.649%

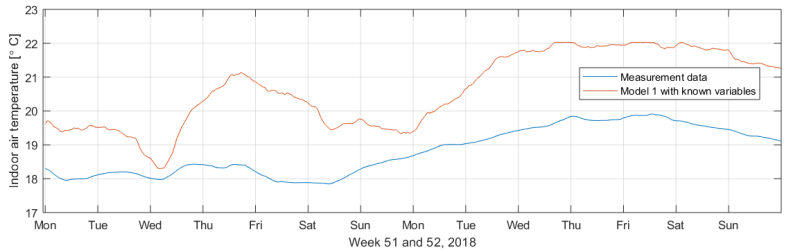

Figure 7.3: Indoor air temperatures for model 1

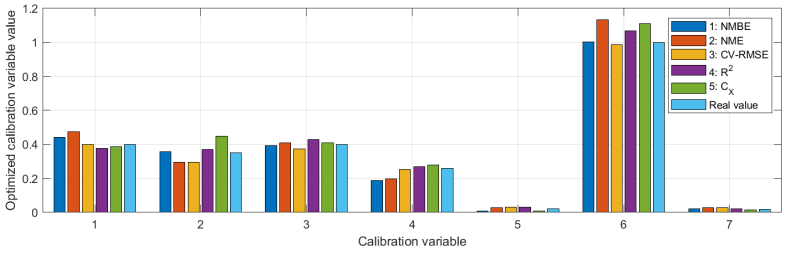

Figure 7.4: Optimal values for calibration variables for model 1

7.3 Model 2

In the second model, the parameters were left constant with exception of the radiator supply temperature. A set point manager with hourly supply temperatures yielded by measurement data was inserted between the hot water source and the radiator. In real buildings, radiator heating systems with a ground source heat pump as the heating source are subject to a variety of errors caused by both aleatory and epistemic uncertainty. These errors may result from a malfunction in the thermostatic valves, a lower heat pump COP than the rated design COP, malfunction in the thermal storage tank, insulation cracks in the piping or tank, missing information about the configuration, among other sources. When modelling this HVAC system in a building energy model, these errors may slip under the radar if not detected. Table 7.3 show that model 2 yielded the lowest SMAPE value so far, with the R^2 function scoring 0.665% for the optimal calibration result. The low relative SMAPE shows that the variables are close to the known values.

Table 7.3: Model 2: Best SMAPE indicators

Error function	*NME*	*NMBE*	*CV(RMSE)*	R^2	C_χ
Optimal SMAPE value	2.095%	1.086%	1.605%	**0.665%**	1.289%
Optimal SMAPE value, relative	38.674%	20.041%	29.615%	12.265%	23.797%

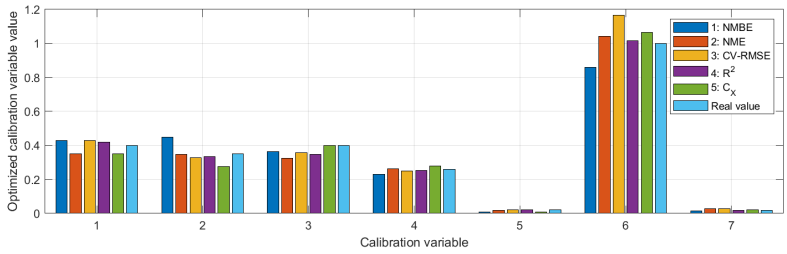

Figure 7.5: Optimal values for calibration variables for model 2

7.4 Model 3

Model 3 can be seen as a different way of approaching model 2. The water radiator is completely removed, replaced by a source of internal gain. The internal gain power is hourly scheduled with values originating from the measured heating power from the radiator. Intuitively, the results from model 2 and model 3 should not vary substantially. However, the optimal SMAPE values do indeed vary. The best error function calibration for model 2 is the worst one for model 3. By looking at figure 7.6 it can be seen that the calibration of the pane conductivity is contributing substantially to this result. The optimal result is seen in table 7.3 being 0.494% for the CV(RMSE) calibration. This score is the best one of the four first model approaches.

Table 7.4: Model 3: Best SMAPE indicators

Error function	*NME*	*NMBE*	*CV(RMSE)*	R^2	C_χ
Optimal SMAPE value	1.303%	1.076%	**0.494%**	2.439%	0.744%
Optimal SMAPE value, relative	24.046%	19.863%	8.477%	45.021%	13.727%

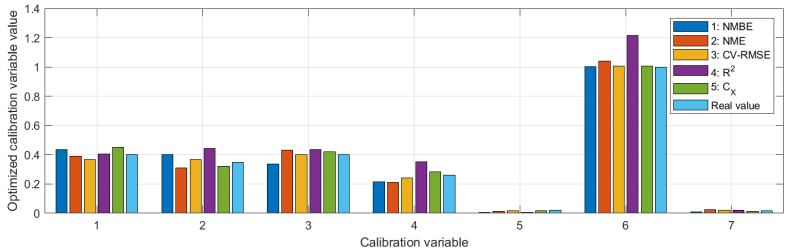

Figure 7.6: Optimal values for calibration variables for model 3

7.5 Model 4

The fourth model keeps all of the variables non-scheduled with exception of the supply temperatures given by the air handling unit. The real supply temperatures were fluctuating around the set point of 19°C, as shown in section 6.3.3. The best SMAPE score for this solution is seen in table 7.5 to be from the NMBE function with 0.697%. The calibrated insulation thickness values are higher for this model, as seen in figure 7.7, which may be a compensation effect caused by the fact that the real AHU supply temperatures were lower for the coldest measured period, week 51. Model 1-4 are combinations where only one parameter at a time is dynamically scheduled. Based on the model results so far, it can be concluded that it is the scheduling of the heating power that has yielded the best result.

Table 7.5: Model 4: Best SMAPE indicators

Error function	*NME*	*NMBE*	*CV(RMSE)*	R^2	C_χ
Optimal SMAPE value	2.407%	**0.697%**	1.496%	1.080%	2.658%
Optimal SMAPE value, relative	44.424%	12.861%	27.607%	19.935%	49.066%

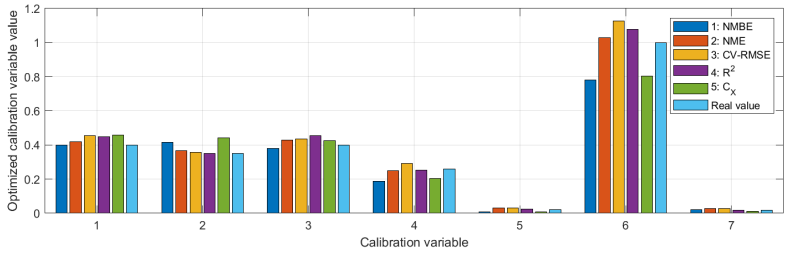

Figure 7.7: Optimal values for calibration variables for model 4

7.6 Model 5

This model represents the solution where both the internal gains and the water radiator supply temperature are scheduled with hourly measurement data. In this manner, the internal heat gains in the model closely represent the actual heat gains for the measurement period. None of the SMAPE indicators reach above 2.0%. This model has the lowest average SMAPE indicator for all of the five optimal solutions, being 1.156%. This can be interpreted as model 5 being the most robust modelling procedure for the calibrated period. Table 7.6 shows the relative R^2-indicator being below 10%, meaning that the calibration reached a value that were within a 10% reach of the exact calibration variable values with respect to the range given by the upper and lower bounds. Figure 7.8 shows that the insulation thicknesses are on average slightly below the real values. Both the infiltration rate and the ventilation rate are slightly higher. This indicates that the modelling procedure with known variables produced higher indoor air temperatures than measured, similar to the case with model 1.

Table 7.6: Model 5: Best SMAPE indicators

Error function	*NME*	*NMBE*	*CV(RMSE)*	R^2	C_χ
Optimal SMAPE value	1.900%	1.286%	1.291%	**0.491%**	0.813%
Optimal SMAPE value, relative	35.065%	23.733%	23.819%	9.071%	15.009%

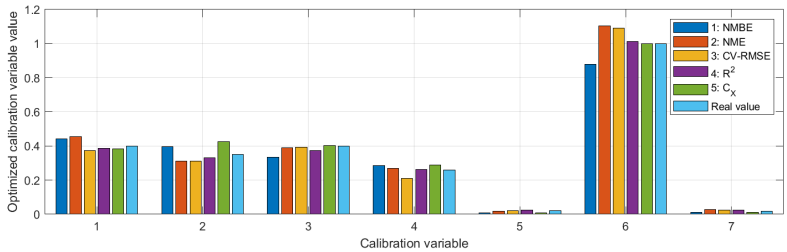

Figure 7.8: Optimal values for calibration variables for model 5

7.7 Model 6

In model 6, the water radiator was removed and replaced as scheduled internal gain. In addition, the air handling unit supply temperature was hourly scheduled. Table 7.7 shows the CV(RMSE) error function yielding the best calibration, being 1.136%. Figure 7.9 shows that the optimized calibration variables are fluctuating more with this approach. This may be caused by the static modelling of the internal gains from the sockets.

Table 7.7: Model 6: Best SMAPE indicators

Error function	*NME*	*NMBE*	*CV(RMSE)*	R^2	C_χ
Optimal SMAPE value	2.090%	1.640%	**1.136%**	1.418%	1.386%
Optimal SMAPE value, relative	38.566%	30.267%	20.975%	26.166%	25.589%

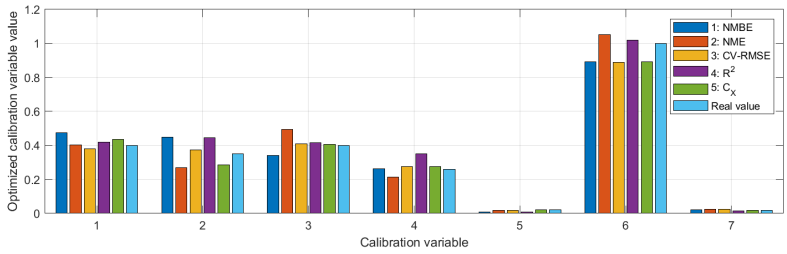

Figure 7.9: Optimal values for calibration variables for model 6

7.8 Model 7

This modelling represents the solution where the internal gains and the AHU supply temperatures are hourly scheduled. The results are overall good, with the highest SMAPE indicator being 1.502% for the C_{χ^2} error function as shown in table 7.8. The water radiator is modelled with no dynamic scheduling, making these results interesting as the radiator is the biggest heat gain source in the model and hereby the potential biggest cause of modelling errors. However, the optimal SMAPE scores with hourly scheduling for the radiator are indeed better as shown in the previous models' results.

Table 7.8: Model 7: Best SMAPE indicators

Error function	*NME*	*NMBE*	*CV(RMSE)*	R^2	C_χ
Optimal SMAPE value	1.307%	1.220%	**1.076%**	1.490%	1.502%
Optimal SMAPE value, relative	24.120%	22.521%	19.861%	27.504%	27.715%

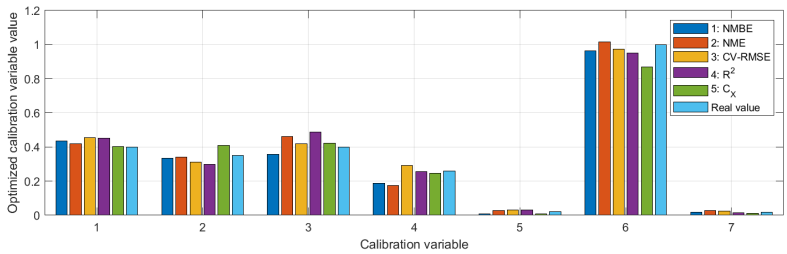

Figure 7.10: Optimal values for calibration variables for model 7

7.9 Model 8

This model contains hourly schedules for internal gains, AHU supply temperatures and the water radiator supply temperature. During the modelling process, this setup was thought to bring the best results, as all of the dynamic variables were hourly scheduled. The best SMAPE indicator was 0.700%, given by calibrating with C_{χ^2} as the objective function, seen in table 7.9. Figure 7.11 shows that the infiltration rate and insulation thicknesses are lower and the mechanical air supply is higher than the real values for this solution. Lowering both the infiltration rate and the insulation thicknesses will potentially yield cancellation effects.

Table 7.9: Model 8: Best SMAPE indicators

Error function	*NME*	*NMBE*	*CV(RMSE)*	R^2	C_χ
Optimal SMAPE value	1.815%	2.071%	2.112%	1.120%	**0.700%**
Optimal SMAPE value, relative	33.505%	38.216%	38.974%	20.667%	12.928%

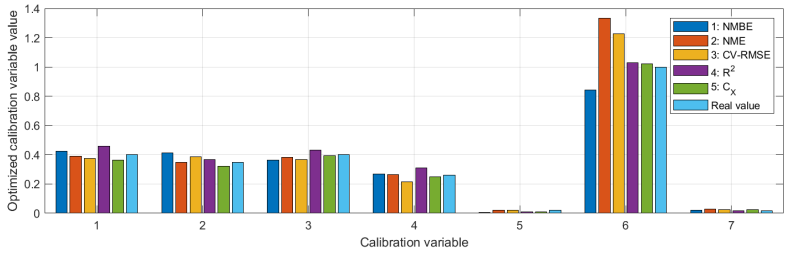

Figure 7.11: Optimal values for calibration variables for model 8

7.10 Model 9

This model contains hourly schedules for the dynamic variables as in model 8, but the water radiator is replaced with internal gains. The optimal SMAPE was given by the use

of CV(RMSE) as the error function, being 0.715%. The optimal insulation thicknesses are on average a good match in terms of the real thicknesses. The infiltration rate is lower, whereas the ventilation rate is higher. The ventilation air temperature is preheated to approximately 19°C before entering the zone, leaving the infiltration rate as the biggest contributor to decreases in the indoor air temperature.

Table 7.10: Model 9: Best SMAPE indicators

Error function	*NME*	*NMBE*	*CV(RMSE)*	R^2	C_χ
Optimal SMAPE value	3.358%	0.853%	**0.715%**	3.026%	0.995%
Optimal SMAPE value, relative	61.973%	15.738%	13.205%	55.846%	18.355%

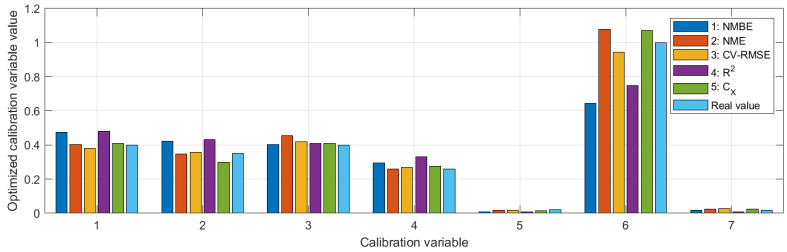

Figure 7.12: Optimal values for calibration variables for model 9

7.11 Best result

Figure 7.13 shows the percentage discrepancy between the known calibration variable values and the given values from the solution with the lowest overall SMAPE value, model 5 with R^2 as the objective function. The mean absolute percentage error (MAPE) was found to be 11.56%. It was shown that the model was producing higher indoor air temperatures than measured with known values, as the insulation thicknesses are lower and both infiltration and ventilation rates are higher for the calibrated values. This was further investigated by plotting the air temperatures represented in figure 7.14. The graph shows that the optimal solution produced lower temperatures than measured, raising a question as to whether the number of simulation runs chosen were sufficient. This was an interesting find, as the genetic algorithm in the calibration process ran a total of 980 simulations for each error function in the model, with a maximum number of generations of 35. This amount of generations may have been insufficient to reach the best match for the calibration variables.

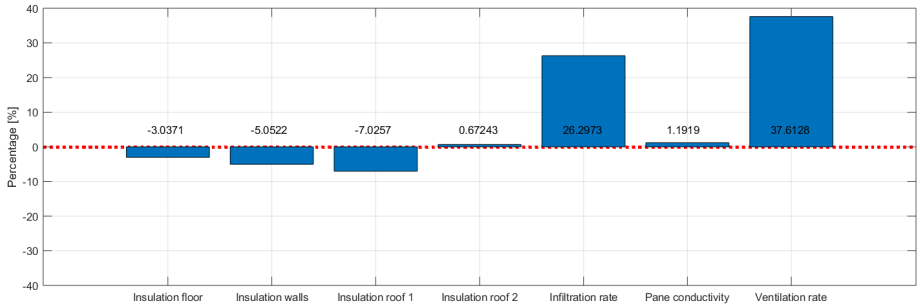

Figure 7.13: Percentage discrepancy plot for optimal solution

The CV(RMSE) score of the key performance indicator was found to be 3.802%. The dotted red line in the plot represents the temperature distribution for model 5 with the known values for the calibration values. This solution is visibly a better match for the measured data. The CV(RMSE) score was also calculated for this solution, yielding 2.441%.

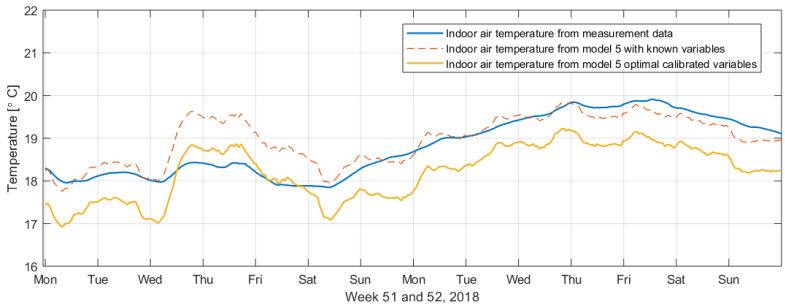

Figure 7.14: Indoor temperature distribution for best model

7.12 Overall evaluation

Table 7.11 summarizes the findings. An interesting find is that for some models, the simulations where the known values of the calibration variables were used yielded a better CV(RMSE) score than simulations with the optimized calibration variables. This is the case for model 0, model 5 and model 8. The multi-objective optimization algorithm was not able to reach a better KPI result by calibrating the selected variables, although a recommended amount of simulations were performed. For the other models, the post-optimization evaluations of the models were better than the pre-optimization evaluations. This means that the adjustment of calibration variables within the allowed range yielded better results than using the real values. This may be interpreted as weaknesses in the models, where the calibration variables were used to compensate for errors originated elsewhere in the model. An important find is that the SMAPE indicator for all of the mod-

els with hourly scheduled modelling of dynamic parameters turned out better than for the base case.

Table 7.11: Total evaluation of the optimized calibration parameters

	CV(RMSE) for KPI with known variables	Best SMAPE indicator for optimized calibration variables	CV(RMSE) for KPI with calibrated variables
Model 0	10.173%	1.343%	16.144%
Model 1	10.212%	0.721%	3.949%
Model 2	2.314%	0.665%	2.210%
Model 3	2.314%	0.494%	4.237%
Model 4	10.074%	0.697%	4.372%
Model 5	2.441%	0.491%	3.802%
Model 6	5.600%	1.136%	3.708%
Model 7	10.120%	1.076%	4.086%
Model 8	2.229%	0.700%	6.957%
Model 9	5.687%	0.715%	4.017%

7.13 General discussion

By looking at the Pareto solution plots in the appendix part 9.2, it is evident that the majority of the models performed well in terms of the fitness function scores. It must be kept in mind that the indoor temperature as the key performance indicator is sensitive to discrepancies compared to for instance energy used for heating/cooling. As an illustration, an example of a building with a measured constant indoor temperature of 21°C is used. A 10% discrepancy between simulated and measured temperature could signify that a building energy model produces an indoor temperature of 18.9°C or 23.1°C. Although the key performance indicator scores within a $\pm$10% range of the real value, it may not be considered a good estimation of reality.

It was interesting to find that the approach where the water supply temperature for the radiator was hourly scheduled, produced more correct calibrated variables than the solution where the radiator is replaced as internal gains., The same rate was chosen for convective and radiative heat and the two solutions were producing correspondent dynamic heating power during test simulations. For the genetic algorithm, the modelling procedure itself can be considered as a black box. The objective functions produces populations of calibration variables by looking at the subsequent key performance indicator error function scores, yielded by the previous generations. The calibration is based on an output evaluation with regards to the variation of input parameters. In this regard, the model simulation process itself is not an influencing factor.

The overall low SMAPE values for the optimal solutions are partly a consequence of the rather strict upper and lower bound chosen as the calibration variable range. The limits were chosen based on estimations of uncertainty when evaluating unknown building parameters. $\pm$10 cm for the insulation thickness in the building envelope was considered a generous range, as well as $\pm$ 55% change in the air flow rate and a $\pm$40% change in the

infiltration rate. The instantaneous infiltration rate of a building is a function of dynamic wind conditions. The nominal infiltration rate of $0.3\ AC/h$ was used as a known calibration variable, even though the actual infiltration rate during the measurement period is unknown. The wind conditions in the simulations were extracted from Voll weather station as opposed to Living Lab. This may be accounted as a source of uncertainty.

Cancellation effects were seen with several of the solutions, where the optimized model had both increased insulation thicknesses and an increased infiltration rate and/or mechanical ventilation rate. As described, the black box approach of the input/output from the simulations made these errors indistinguishable for the objective functions. To minimize this effect, either the amount of calibration variables could have been reduced, or the calibration variables should have yielded the same effect on the indoor temperature, namely a reduction or an increase. Compensation effects are also evident by looking at the overall better performance of the KPI with calibrated parameters compared to the KPI with the known value of the parameters. This compensation effect is not distinguishable when the actual calibration variable values are unknown. In this case study, the thermal bridge values were not chosen as calibration variables due to the uncertainty of the actual values. It was seen in the optimal solution that all of the calibrated variables were contributing to a lower indoor air temperature, which may be interpreted as a compensation for other parameters in the model. For instance, thermal bridge values may have been set too low.

The risk of over-fitting is always present in building energy model calibration. In practice this means that the building model is adjusted to fit a specific set of measurement data but may perform poorly when calibrated against another set of measurement data. The modelling of dynamic parameters by hourly scheduling from measurement data can be seen as a form of over-fitting, as the model would need to implement these measurements for each calibrated period. The scope of the simulations was to extract the value of assumed unknown building parameters, by using building energy modelling calibration as a means to an end. Hence, none of the models may be considered as calibrated for scenarios deviating from the measurement period.

The main finding to be extracted from the results is that modelling dynamic parameters like heating power, internal gains and supply temperatures from the air handling unit with exact hourly values indeed produced better results in terms of the optimization-based calibration of the chosen variables. The SMAPE indicators in table 7.11 show that model 0 with no dynamic modelling produced the highest discrepancy between known calibration variable values and optimized values. However, the access to this kind of measurement data may not be as straight-forward as for the case with Living Lab, being a test facility. When it comes to buildings with direct electric heating, there are ways to approach this solution without using earmarked energy meters. The majority of the electricity use in Norwegian households during winter periods originates from heating. From the start of 2019, all Norwegian households have installed smart energy meters (AMS) that monitors hourly energy consumption. Tests may be performed to find the base consumption without heating appliances on. In a winter period, this consumption may be subtracted from the total energy consumption, yielding an approximate energy use left for heating. This heating can be inserted as hourly scheduled gain in a building energy model.

Chapter 8

Conclusion

The methodology adopted for investigating unknown building parameters revealed that the best results were reached when the dynamic parameters were modelled from exact measurement data. This finding corresponded with initial assumptions. The chosen building is a test facility with an HVAC system that may be considered as complex compared to most Norwegian residential buildings. A solution where important heat gain parameters are extracted directly from measurements as opposed to being modelled by the user requires less skill and experience. For this reason it may be a good modelling approach when the aim is to investigate unknown building parameters. A downfall with this method is that the building energy modeller needs access to measurement data that may be unavailable or difficult to obtain.

It was seen that the best solution originated from model 5 could have reached an even better calibration result. The genetic algorithm procedure was stopped after a maximum amount of 35 generations with a population size of 28. This amount of generations could have been set higher to see whether the algorithm would have performed better.

This thesis has been a qualitative case study, which prohibits the drawing of general conclusions. Nevertheless, the case study showed that a scheduled modelling of dynamic parameters taken from measurement data contributed to a more accurate calibration of the selected building parameters.

Chapter 9

Future work

Below is a list with recommendations for future work within the field of employing optimization-based calibration tools to find unknown parameters in building energy models.

1. When the key performance indicator is temperature, do a separate calibration of variables that may have cancellation effects in terms of the evaluation of the key performance indicator. This may be for instance building envelope U-value components and infiltration/ventilation rates.

2. Test the multi-objective optimization procedure on a building with direct electric heating. The heating power could be modelled dynamically with measured data, and as a function of the thermostatic control system.

3. Increase the number of simulation runs to check whether it affects the calibration outputs.

4. Further evaluate the optimization-based algorithm by continuing the testing on other buildings, as well as testing it for longer calibration periods.

Bibliography

Asadi, S., Mostavi, E., Boussaa, D., Indaganti, M., 2019. Building Energy Model Calibration Using Automated Optimization-Based Algorithm. Energy and Buildings 198, 106–114.
URL https://linkinghub.elsevier.com/retrieve/pii/S0378778819303330

Augenbroe, G., 2011. The role of simulation in performance based building. In: Hensen, J. L. M., Lamberts, R. (Eds.), Building Performance Simulation for Design and Operation. Spon Press, London and New York, Ch. 2, pp. 15–36.

Big Ladder Software, 2019. Elements.
URL https://bigladdersoftware.com/projects/elements/

Bird, R. E., Riordan, C., 2002. Simple Solar Spectral Model for Direct and Diffuse Irradiance on Horizontal and Tilted Planes at the Earth's Surface for Cloudless Atmospheres. Journal of Climate and Applied Meteorology 25 (1), 87–97.

Carlucci, S., 2019. Living Lab - A ZEB-pilot project at NTNU [presentation].
URL https://ntnu.blackboard.com/bbcswebdav/pid-551447-dt-content-rid-19868201_1/courses/194_TBA4166_1_2019_V_1/ZEB_LivingLab_Projectdescription.pdf

Claridge, D. E., 2011. Building simulation for practical operational optimization. In: Hensen, J. L. M., Lamberts, R. (Eds.), Building Performance Simulation for Design and Operation. Spon Press, London and New York, Ch. 13, pp. 365–401.

de Beer, J., 2017. Ground Sourced Energy.
URL https://www.ngu.no/en/topic/ground-sourced-energy

Dupont Energain, 2010. Energy-saving thermal mass systems [brochure].

European Union, 2019. About Copernicus.
URL https://www.copernicus.eu/en/about-copernicus

Ferrari, S., Zanotto, V., 2016. Building Energy Performance Assessment in Southern Europe. Springer, Milano.

Garrett, A., New, J., 2016. Suitability of ASHRAE Guideline 14 Metric for Calibration. ASHRAE Trans.; (United States) 037 (OR-16), 469–477.

Geem, Z. W., Kim, J. H., 2001. A New Heuristic Optimization Algorithm: Harmony Search. Simulation 76 (2), 60:68.

Global Alliance for Buildings and Construction, 2019. 2018 GLOBAL STATUS REPORT. URL https://architecture2030.org/buildings_problem_why/

Goia, F., Finocchiaro, L., Gustavsen, A., 2015. The ZEB Living Laboratory at the Norwegian University of Science and Technology : a zero emission house for engineering and social science experiments. 7. Passivhus Norden — Sustainable Cities and Buildings (7th), 20–21.

Google Maps, 2019. Distance between ZEB Living Lab and Voll weather station. URL https://www.google.com/maps/@63.4146447,10.4282944,14z

Haug, K. B., 2018. Energy-related occupant behavior – Movement monitoring [project thesis].

He, Y., Mirzargar, M., Kirby, R. M., 2015. Mixed aleatory and epistemic uncertainty quantification using fuzzy set theory. International Journal of Approximate Reasoning 66, 1–15.

Henninger, R. H., Witte, M. J., 2004. EnergyPlus testing with ANSI/ASHRAE standard 140-2001 (BESTEST) 2001 (June), 1–91.

Hensen, J. L. M., Lamberts, R., 2011. Building Performance Simulation for Design and Operation. Spon Press, London and New York.

Heo, Y., Choudhary, R., Augenbroe, G. A., 2012. Calibration of building energy models for retrofit analysis under uncertainty. Energy and Buildings 47, 550–560.

Kennedy, J., Eberhart, R., 1995. Particle Swarm Optimization. Proceedings of IEEE International Conference on Neural Networks (ICNN) 4.

Khoury, J., Alameddine, Z., Hollmuller, P., 2017. Understanding and bridging the energy performance gap in building retrofit. Energy Procedia 122, 217–222. URL https://doi.org/10.1016/j.egypro.2017.07.348

Lara, R. A., Pernigotto, G., Zhang, Y., Barzon, F., Gasparella, A., Romagnoni, P., Cappelletti, F., Naboni, E., 2017. Optimization Tools for Building Energy Model Calibration. Energy Procedia 111 (September 2016), 1060–1069. URL http://dx.doi.org/10.1016/j.egypro.2017.03.269

Lyngson, 2005. Brochure: LUDVIG menneskelig varme.

Monetti, V., Davin, E., Fabrizio, E., André, P., Filippi, M., 2015. Calibration of building energy simulation models based on optimization: A case study. Energy Procedia 78, 2971–2976.
URL http://dx.doi.org/10.1016/j.egypro.2015.11.693

Mustafaraj, G., Marini, D., Costa, A., Keane, M., 2014. Model calibration for building energy efficiency simulation. Applied Energy 130, 72–85.
URL http://dx.doi.org/10.1016/j.apenergy.2014.05.019

National Research Council, 2012. Assessing the Reliability of Complex Models: Mathematical and statistical foundations of verification, validation, and uncertainty quantification. Tech. rep., National Academies Press, Washington D.C.
URL http://scholar.google.com/scholar?hl=en&btnG=Search&q=intitle:Assessing+the+Reliability+of+Complex+Models:+Mathematical+and+Statistical+Foundations+of+Verification,+Validation,+and+Uncertainty+Quantification#0%0Ahttp://www.nap.edu/catalog/13395

Norwegian Meteorological Institute, 2019. eKlima.
URL http://sharki.oslo.dnmi.no/portal/page?_pageid=73,39035,73_39049&_dad=portal&_schema=PORTAL

NTNU Department of Archtecture and Technology, 2019. Sustainable Architecture [image].
URL https://www.ntnu.edu/studies/mssusarc

Pedersen, A. S., 2018. Moisture production in buildings [Master thesis] (August).

Rajendra, K., 2017. Heat and Mass Transfer, ebook Edition. No. September 2005. Springer Nature, Jodhpur, Rajasthan, India.

Ramos Ruiz, G., Fernández Bandera, C., Gómez-Acebo Temes, T., Sánchez-Ostiz Gutierrez, A., 2016. Genetic algorithm for building envelope calibration. Applied Energy 168, 691–705.

Reddy, T. A., 2006. Literature Review on Calibration of Building Energy Simulation Programs : Uses , Problems , Procedur ... ASHRAE Transactions (112), 226.

Rohdin, P., Molin, A., Moshfegh, B., 2014. Experiences from nine passive houses in Sweden - Indoor thermal environment and energy use. Building and Environment 71, 176–185.
URL http://dx.doi.org/10.1016/j.buildenv.2013.09.017

Royapoor, M., Roskilly, T., 2015. Building model calibration using energy and environmental data. Energy and Buildings 94, 109–120.
URL http://dx.doi.org/10.1016/j.enbuild.2015.02.050

Ruiz, G. R., Bandera, C. F., 2017. Validation of calibrated energy models: Common errors. Energies 10 (10).

SINTEF Byggforsk, 2019. Hva er Byggforskserien.
URL https://www.byggforsk.no/side/198/hva_er_byggforskserien

Slanzi, D., Borrotti, M., De March, D., Orlando, D., Giove, S., Poli, I., 2014. Qualitative Particle Swarm Optimization (Q-PSO) for Energy-Efficient Building Designs. In: Advances in Artificial Life and Evolutionary Computation. Springer Cham, pp. 13–26.

Spitler, J. D., 2011. Thermal load and energy performance prediction. In: Hensen, J. L. M., Lamberts, R. (Eds.), Building Performance Simulation for Design and Operation. Spon Press, London and New York, Ch. 5, pp. 84–142.

Tian, W., Heo, Y., de Wilde, P., Li, Z., Yan, D., Park, C. S., Feng, X., Augenbroe, G., 2018. A review of uncertainty analysis in building energy assessment. Renewable and Sustainable Energy Reviews 93, 285–301.

Vogler-Finck, P., Clauß, J., Georges, L., 2017. A Dataset To Support Dynamical Modelling Of The Thermal Dynamics Of A Super-Insulated Building (1), 1–28.
URL https://zenodo.org/record/1034820#.Wf2mMBO0NTZ

Vogt, M., Remmen, P., Lauster, M., Fuchs, M., Müller, D., 2018. Selecting statistical indices for calibrating building energy models. Building and Environment 144 (August), 94–107.
URL https://doi.org/10.1016/j.buildenv.2018.07.052

Waters, J. R., 2003. Energy conservation in buildings: a guide to Part L of the Building regulations. Oxford.

Wiik, M. K., 2017. Life Cycle GHG Emissions of Material Use in the Living Laboratory. No. June 2016.

Appendix

9.1 MATLAB script for CV(RMSE) analysis of KPI

```
1
2  %%Calibration test of models with known calibration
       variable values,
3  %%pre-optimization
4
5  %Plot:
6  File1 = 'LivingLab_week_5152.csv';
7  simulated = csvread(File1,1,1);
8  optimT = simulated(:,4);
9  measuredT1 = ObservedData2(:,1);
10 measuredT2 = ObservedData3(:,1);
11 totmeasured = [measuredT1;measuredT2];
12
13 figure (1)
14 plot(totmeasured)
15 hold on
16 grid on
17 plot(optimT)
18 legend('Measurement data', ...
19     'Model X with known variables');
20 t=1:336;
21 set(gca,'xtick',linspace(t(1),t(end),15))
22 week = {'Mon','Tue','Wed','Thu','Fri','Sat','Sun', ...
23     'Mon','Tue','Wed','Thu','Fri','Sat','Sun',' '};
24 xticklabels(week)
25 xlabel('Week 51 and 52, 2018');
26 ylabel('Indoor air temperature [\circ C]');
27 xlim([0 336]);
28 set(gcf, 'Position',  [1, 1, 1100, 300])
29 saveas(gcf,'PreCalibrationX.png');
30
31 %Evaluation of CV(RMSE):
32 diff = totmeasured - optimT;
33 diff_squared = (diff).^2;
34 n = length(totmeasured);
35 diffsum = sum(diff_squared);
36 tobesquared = diffsum/n;
37 mean_measured = mean(totmeasured);
```

```
38
39 CVRMSE(1) = sqrt(tobesquared)/mean_measured * 100
40
41 %Calibration test of model with optimized calibration
       variables according
42 %to SMAPE indicator
43
44 %Plot:
45 File2 = 'LivingLab_week_5152opt.csv';
46 simulated = csvread(File2,1,1);
47 optimT2 = simulated(:,4);
48 measuredT1 = ObservedData2(:,1);
49 measuredT2 = ObservedData3(:,1);
50 totmeasured = [measuredT1;measuredT2];
51
52 figure (2)
53 plot(totmeasured)
54 hold on
55 grid on
56 plot(optimT2)
57 legend('Measurement data', ...
58     'Model X with optimized calibrated variables');
59 t=1:336;
60 set(gca,'xtick',linspace(t(1),t(end),15))
61 week = {'Mon','Tue','Wed','Thu','Fri','Sat','Sun', ...
62     'Mon','Tue','Wed','Thu','Fri','Sat','Sun',' '};
63 xticklabels(week)
64 xlabel('Week 51 and 52, 2018');
65 ylabel('Indoor air temperature [\circ C]');
66 xlim([0 336]);
67 %ylim([16 22]);
68 set(gcf, 'Position', [1, 1, 1100, 300])
69 saveas(gcf,'PostCalibrationX.png');
70
71 %Evaluation of CV(RMSE):
72 diff = totmeasured - optimT2;
73 diff_squared = (diff).^2;
74 n = length(totmeasured);
75 diffsum = sum(diff_squared);
76 tobesquared = diffsum/n;
77 mean_measured = mean(totmeasured);
78
79 CVRMSE(2) = sqrt(tobesquared)/mean_measured * 100
```

9.2 MATLAB script for SMAPE analysis and Pareto frontiers

```
%% Analysis of results
%Below is the script written to enable the presentation of the results
% from the multi-objective optimization.
% The fitness values from the pareto solutions were saved in a struct
% called "Name_fitness_values". The corresponding calibration variables
% were saved in a struct called "Name_bestpoints".

%% Individual SMAPE indicators for each Pareto-optimal solution

%NMBE:
CV1_bestpoints_nmbe = Name_bestpoints{1,1}(:,1);
ParetoNMBE(:,:) = Name_bestpoints{1,1}(:,:);
n_nmbe = length(CV1_bestpoints_nmbe);

for count = 1:n_nmbe

CorrectValues(count,:) = [0.4,0.35,0.4,0.26,0.019647,1,0.01833];
DiffNMBE(count,:) = ParetoNMBE(count,:) - CorrectValues(count,:);
DiffAbsNMBE = abs(DiffNMBE);

PlusAbsNMBE(count,:) = abs(ParetoNMBE(count,:)) + CorrectValues(count,:);
PlusAbsDivNMBE(count,:) = PlusAbsNMBE(count,:) ./ 2;

SumDiffAbsNMBE = sum(DiffAbsNMBE(count,:));
SumPlusAbsDivNMBE = sum(PlusAbsDivNMBE(count,:));
SMAPE_NMBE(count) = (1/nvar) * (SumDiffAbsNMBE/SumPlusAbsDivNMBE) * 100;

     SumDiffAbsNMBE = [];
     SumPlusAbsDivNMBE = [];

end

%NME:
CV1_bestpoints_nme = Name_bestpoints{2,1}(:,1);
```

```
35 ParetoNME(:,:) = Name_bestpoints{2,1}(:,:);
36 n_nme = length(CV1_bestpoints_nme);
37
38 for count = 1:n_nme
39
40     CorrectValues(count,:) =
           [0.4,0.35,0.4,0.26,0.019647,1,0.01833];
41     DiffNME(count,:) = ParetoNME(count,:) - CorrectValues(
           count,:);
42     DiffAbsNME = abs(DiffNME);
43
44     PlusAbsNME(count,:) = abs(ParetoNME(count,:)) +
           CorrectValues(count,:);
45     PlusAbsDivNME(count,:) = PlusAbsNME(count,:) ./ 2;
46
47     SumDiffAbsNME = sum(DiffAbsNME(count,:));
48     SumPlusAbsDivNME = sum(PlusAbsDivNME(count,:));
49     SMAPE_NME(count) = (1/nvar) * (SumDiffAbsNME/
           SumPlusAbsDivNME) * 100;
50
51     SumDiffAbsNME = [];
52     SumPlusAbsDivNME = [];
53
54 end
55
56 %CV-RMSE:
57 CV1_bestpoints_cv = Name_bestpoints{3,1}(:,1);
58 ParetoCV(:,:) = Name_bestpoints{3,1}(:,:);
59 n_cv = length(CV1_bestpoints_cv);
60
61 for count = 1:n_cv
62
63     CorrectValues(count,:) =
           [0.4,0.35,0.4,0.26,0.019647,1,0.01833];
64     DiffCV(count,:) = ParetoCV(count,:) - CorrectValues(
           count,:);
65     DiffAbsCV = abs(DiffCV);
66
67     PlusAbsCV(count,:) = abs(ParetoCV(count,:)) +
           CorrectValues(count,:);
68     PlusAbsDivCV(count,:) = PlusAbsCV(count,:) ./ 2;
69
70     SumDiffAbsCV = sum(DiffAbsCV(count,:));
71     SumPlusAbsDivCV = sum(PlusAbsDivCV(count,:));
72     SMAPE_CV(count) = (1/nvar) * (SumDiffAbsCV/
```

```
        SumPlusAbsDivCV) * 100;

    SumDiffAbsCV = [];
    SumPlusAbsDivCV = [];

end

%R2:
CV1_bestpoints_r2 = Name_bestpoints{4,1}(:,1);
ParetoR2(:,:) = Name_bestpoints{4,1}(:,:);
n_r2 = length(CV1_bestpoints_r2);

for count = 1:n_r2

    CorrectValues(count,:) =
        [0.4,0.35,0.4,0.26,0.019647,1,0.01833];
    DiffR2(count,:) = ParetoR2(count,:) - CorrectValues(
        count,:);
    DiffAbsR2 = abs(DiffR2);

    PlusAbsR2(count,:) = abs(ParetoR2(count,:)) +
        CorrectValues(count,:);
    PlusAbsDivR2(count,:) = PlusAbsR2(count,:) ./ 2;

    SumDiffAbsR2 = sum(DiffAbsR2(count,:));
    SumPlusAbsDivR2 = sum(PlusAbsDivR2(count,:));
    SMAPE_R2(count) = (1/nvar) * (SumDiffAbsR2/
        SumPlusAbsDivR2) * 100;

    SumDiffAbsR2 = [];
    SumPlusAbsDivR2 = [];

end

%Cchi:
CV1_bestpoints_chi = Name_bestpoints{5,1}(:,1);
ParetoCHI(:,:) = Name_bestpoints{5,1}(:,:);
n_chi = length(CV1_bestpoints_chi);

for count = 1:n_chi

    CorrectValues(count,:) =
        [0.4,0.35,0.4,0.26,0.019647,1,0.01833];
    DiffCHI(count,:) = ParetoCHI(count,:) - CorrectValues(
        count,:);
```

```
111     DiffAbsCHI = abs(DiffCHI);
112
113     PlusAbsCHI(count,:) = abs(ParetoCHI(count,:)) +
            CorrectValues(count,:);
114     PlusAbsDivCHI(count,:) = PlusAbsCHI(count,:) ./ 2;
115
116     SumDiffAbsCHI = sum(DiffAbsCHI(count,:));
117     SumPlusAbsDivCHI = sum(PlusAbsDivCHI(count,:));
118     SMAPE_CHI(count) = (1/nvar) * (SumDiffAbsCHI/
            SumPlusAbsDivCHI) * 100;
119
120     SumDiffAbsCHI = [];
121     SumPlusAbsDivCHI = [];
122
123 end
124
125 %% Plotting of the calibration variables for the best SMAPE
        in a bar plot
126 %Best SMAPE indicator for each error function:
127 x1 = min(SMAPE_NMBE);
128 x2 = min(SMAPE_NME);
129 x3 = min(SMAPE_CV);
130 x4 = min(SMAPE_R2);
131 x5 = min(SMAPE_CHI);
132 bestsmapes = [x1 x2 x3 x4 x5]
133
134 %Array position of best SMAPE value:
135 pos1 = find(SMAPE_NMBE == min(SMAPE_NMBE));
136 pos2 = find(SMAPE_NME == min(SMAPE_NME));
137 pos3 = find(SMAPE_CV == min(SMAPE_CV));
138 pos4 = find(SMAPE_R2 == min(SMAPE_R2));
139 pos5 = find(SMAPE_CHI == min(SMAPE_CHI));
140
141 optval1 = ParetoNMBE(pos1,:);
142 optval2 = ParetoNME(pos2,:);
143 optval3 = ParetoCV(pos3,:);
144 optval4 = ParetoR2(pos4,:);
145 optval5 = ParetoCHI(pos5,:);
146 realval = CorrectValues(1,:);
147
148 figure (1)
149 bpcombo = [optval1(:),optval2(:),optval3(:),optval4(:),
        optval5(:),realval(:)];
150 hb = bar(bpcombo, 'grouped');
151 labels = ['1';'2';'3';'4';'5';'6';'7'];
```

```
set(gca, 'XTick', 1:7, 'XTickLabel', labels)
set(gcf, 'Position', [1, 1, 1100, 300])
xlabel('Calibration variable');
ylabel('Optimized calibration variable value');
grid on
legend('1: NMBE','2: NME','3: CV-RMSE','4: R^2','5: C_X','
    Real value');
saveas(gcf,'Plot_Barplot0.png');

%% Pareto plots

%Collecting the best fitness values from the optimization
    runs
%NMBE:
F1_nmbe = Name_fitness_values{1,1}(:,1);
F2_nmbe = Name_fitness_values{1,1}(:,2);
%NME:
F1_nme = Name_fitness_values{2,1}(:,1);
F2_nme = Name_fitness_values{2,1}(:,2);
%CV-RMSE:
F1_cv = Name_fitness_values{3,1}(:,1);
F2_cv = Name_fitness_values{3,1}(:,2);
%R2:
F1_r2 = Name_fitness_values{4,1}(:,1);
F2_r2 = Name_fitness_values{4,1}(:,2);
%Cchi:
F1_chi = Name_fitness_values{5,1}(:,1);
F2_chi = Name_fitness_values{5,1}(:,2);

%Plotting them in a merged chart
figure (2)
set(gcf, 'Position', [1, 10, 700, 1000])
ax1 = subplot(3,2,1);
x1 = F1_nmbe;
y1 = F2_nmbe;
plot(ax1,x1,y1,'+','LineWidth',2,'Color','r')
grid on
xlabel('Fitness function score 1');
ylabel('Fitness function score 2');
title(ax1,'Pareto solutions: NMBE');
ax2 = subplot(3,2,2);
x2 = F1_nme;
y2 = F2_nme;
plot(ax2,x2,y2,'+','LineWidth',2,'Color','g')
xlabel('Fitness function score 1');
```

```
ylabel('Fitness function score 2');
title(ax2,'Pareto solutions: NME');
grid on
ax3 = subplot(3,2,3);
x3 = F1_cv;
y3 = F2_cv;
plot(ax3,x3,y3,'+','LineWidth',2,'Color','m')
grid on
xlabel('Fitness function score 1');
ylabel('Fitness function score 2');
title(ax3,'Pareto solutions: CV-RMSE');
ax4 = subplot(3,2,4);
x4 = F1_r2;
y4 = F2_r2;
plot(ax4,x4,y4,'+','LineWidth',2,'Color','b')
grid on
xlabel('Fitness function score 1');
ylabel('Fitness function score 2');
title(ax4,'Pareto solutions: R^2');
ax5 = subplot(3,2,5);
x5 = F1_chi;
y5 = F2_chi;
plot(ax5,x5,y5,'+','LineWidth',2,'Color','r')
grid on
xlabel('Fitness function score 1');
ylabel('Fitness function score 2');
title(ax5,'Pareto solutions: C_X');
saveas(gcf,'Plot_Pareto0.png');
```

9.3 Pareto frontiers for the error functions

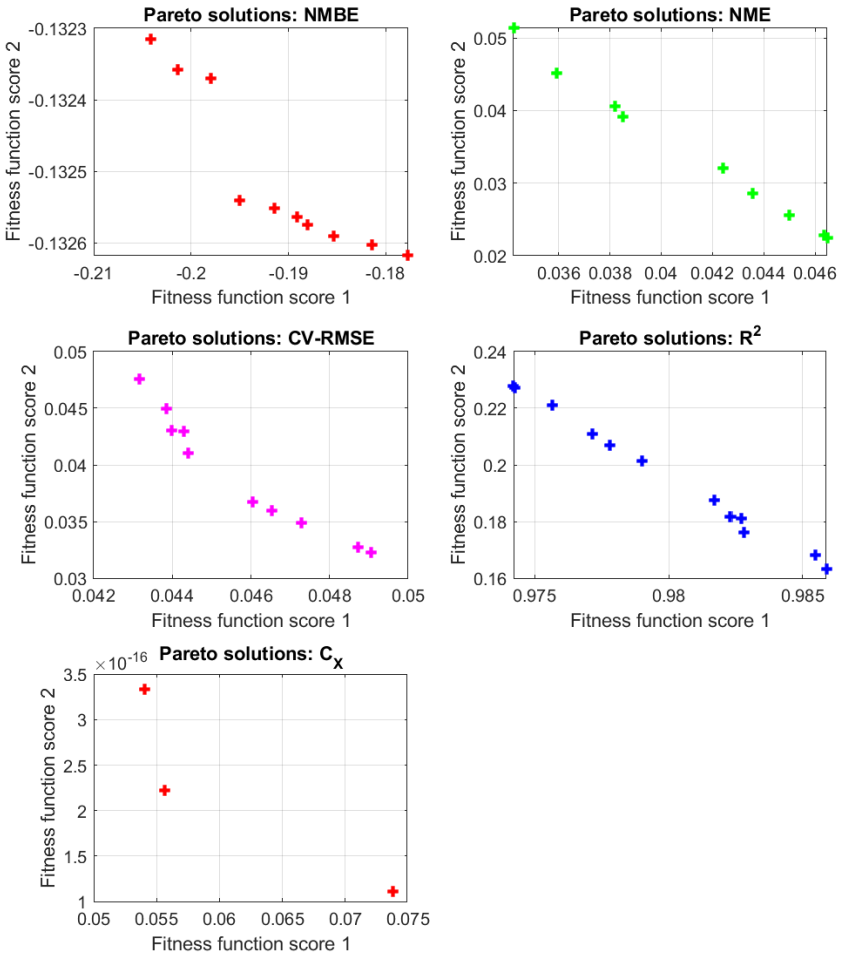

Figure 9.1: Pareto solutions for model 1

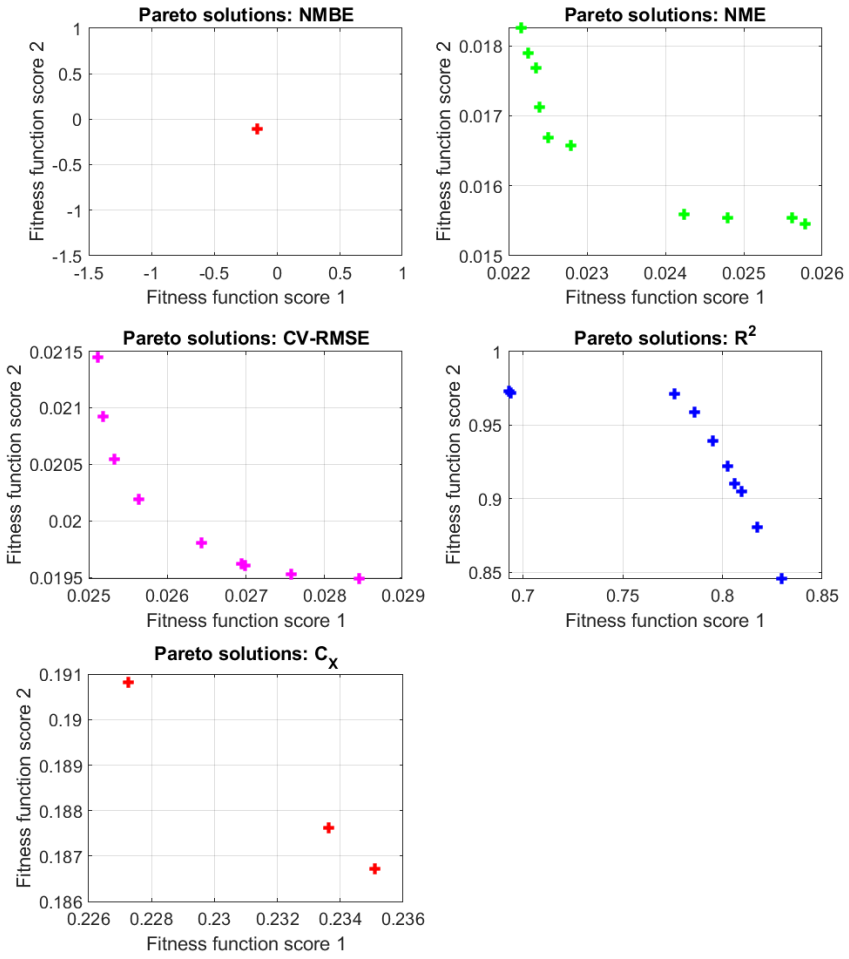

Figure 9.2: Pareto solutions for model 2

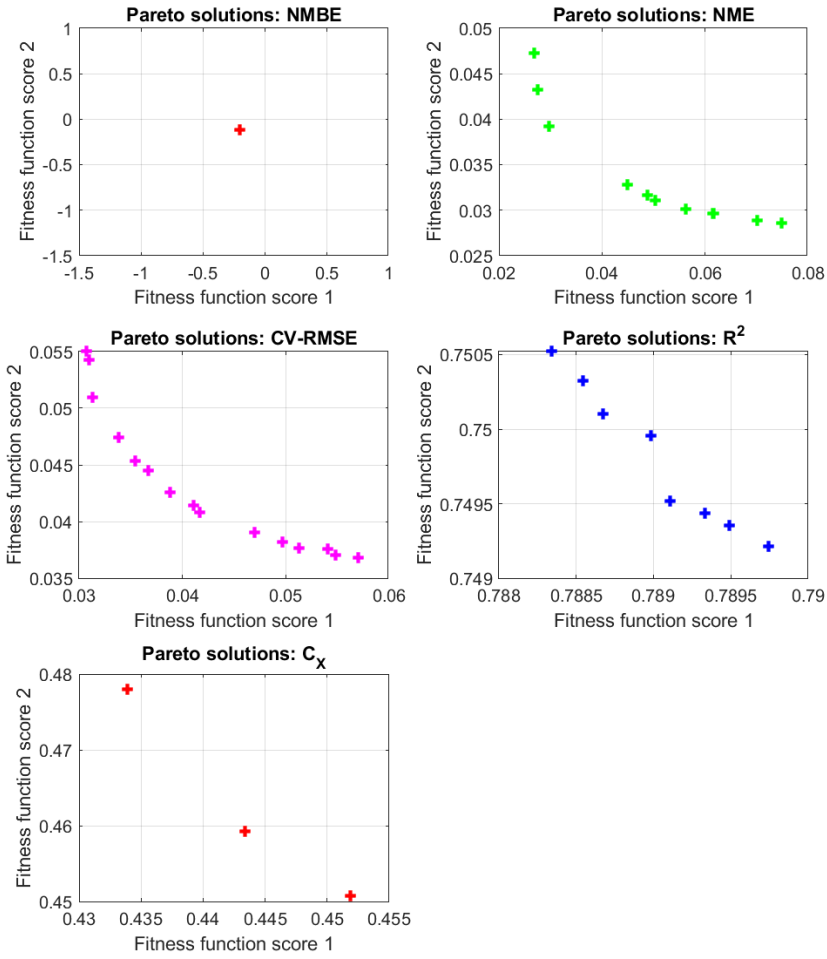

Figure 9.3: Pareto solutions for model 3

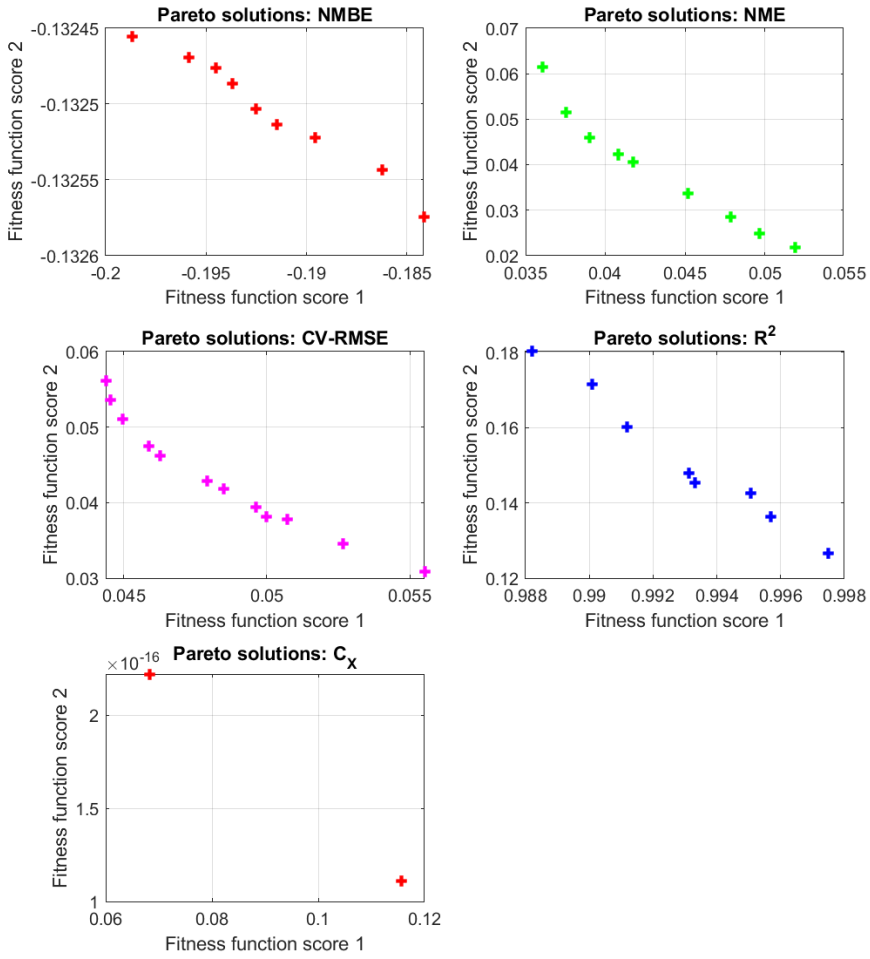

Figure 9.4: Pareto solutions for model 4

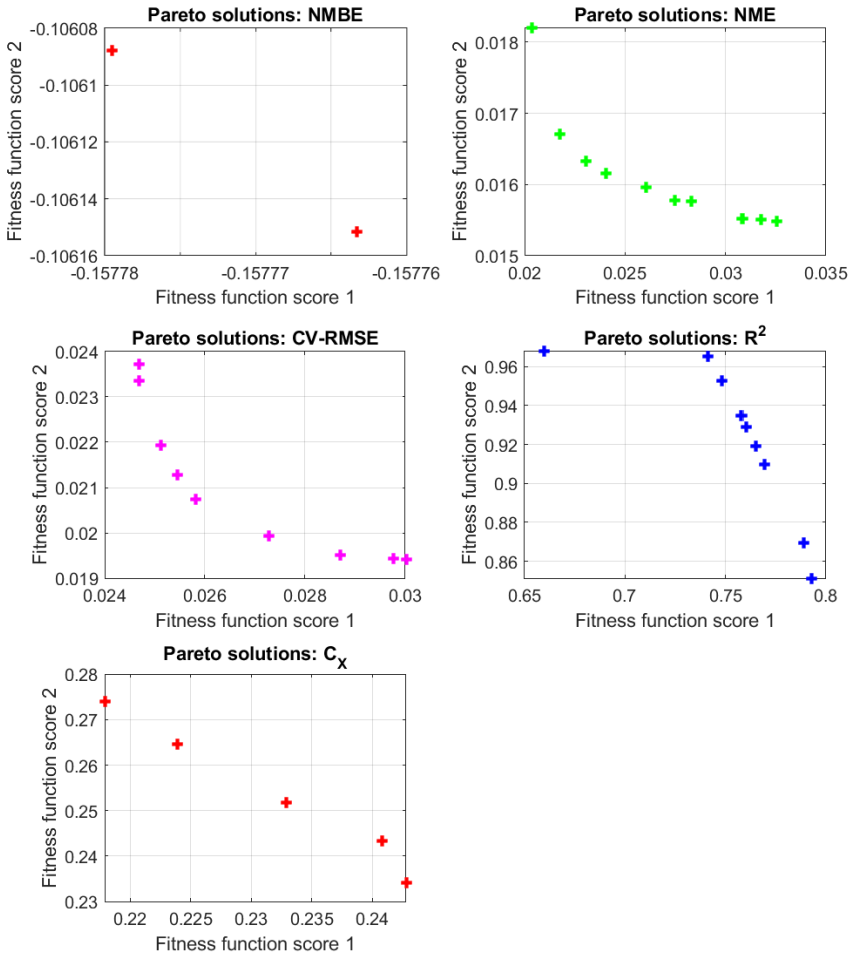

Figure 9.5: Pareto solutions for model 5

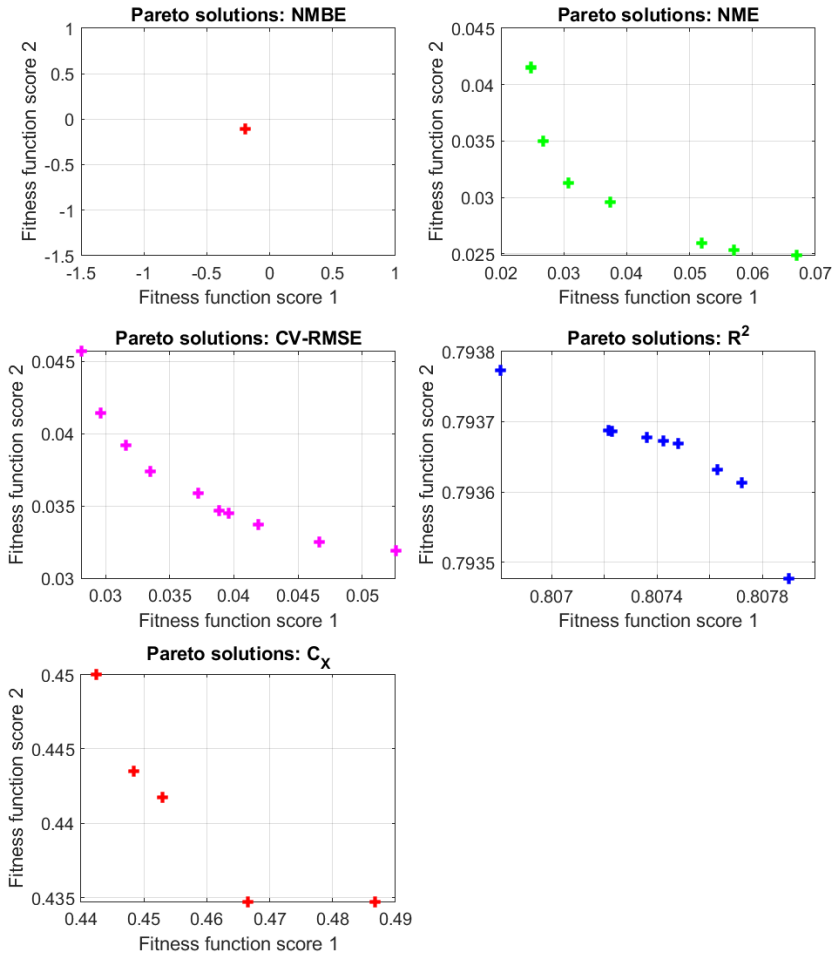

Figure 9.6: Pareto solutions for model 6

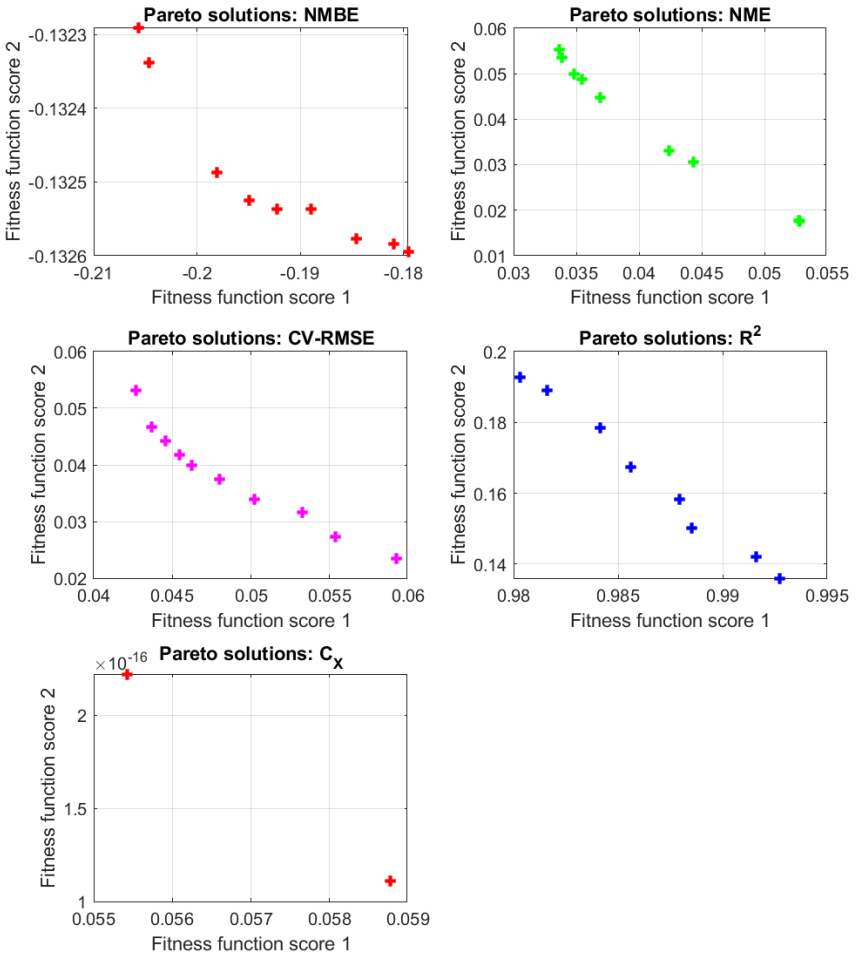

Figure 9.7: Pareto solutions for model 7

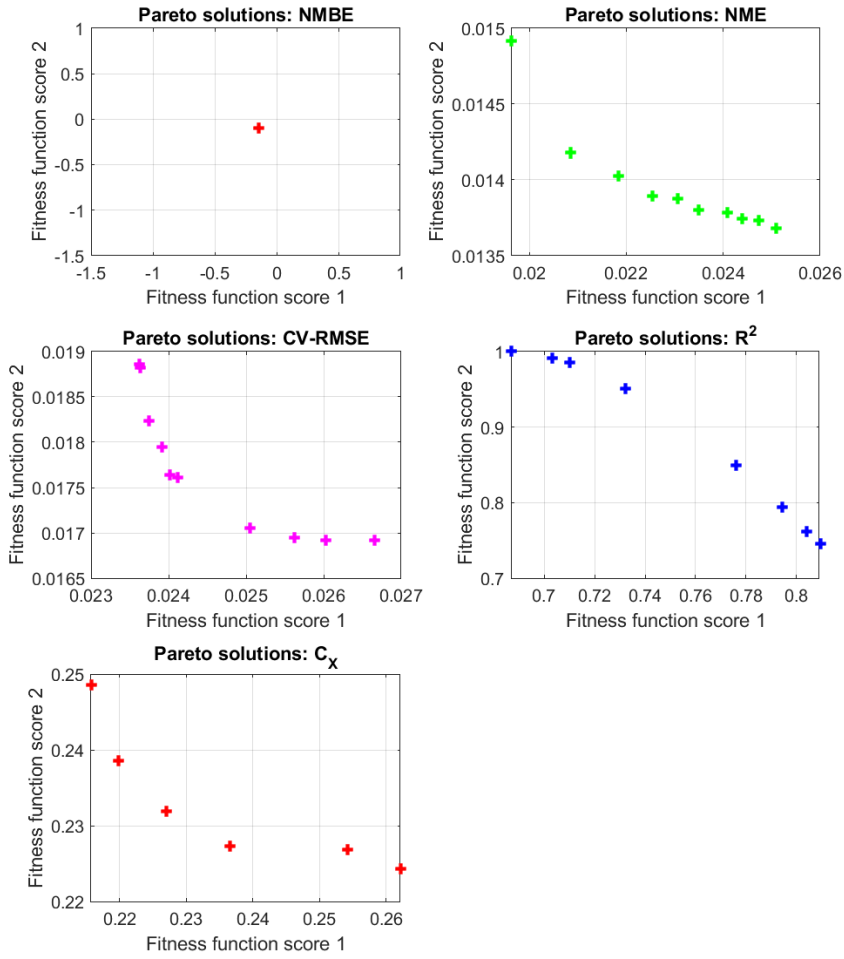

Figure 9.8: Pareto solutions for model 8

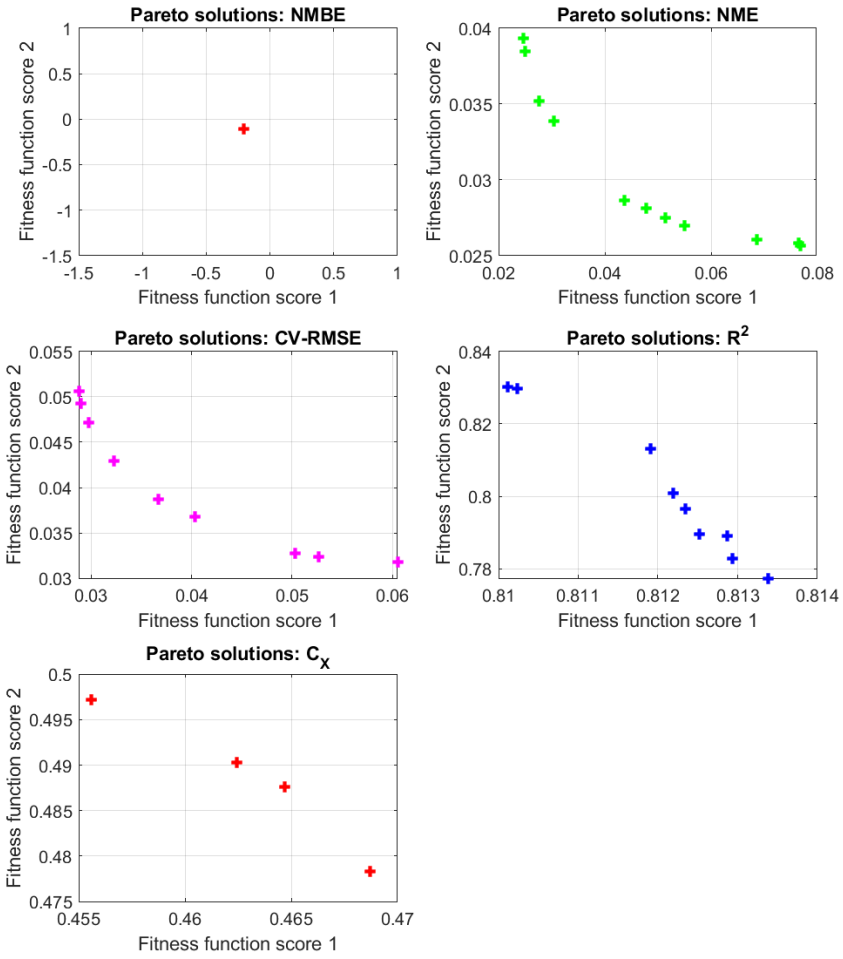

Figure 9.9: Pareto solutions for model 9

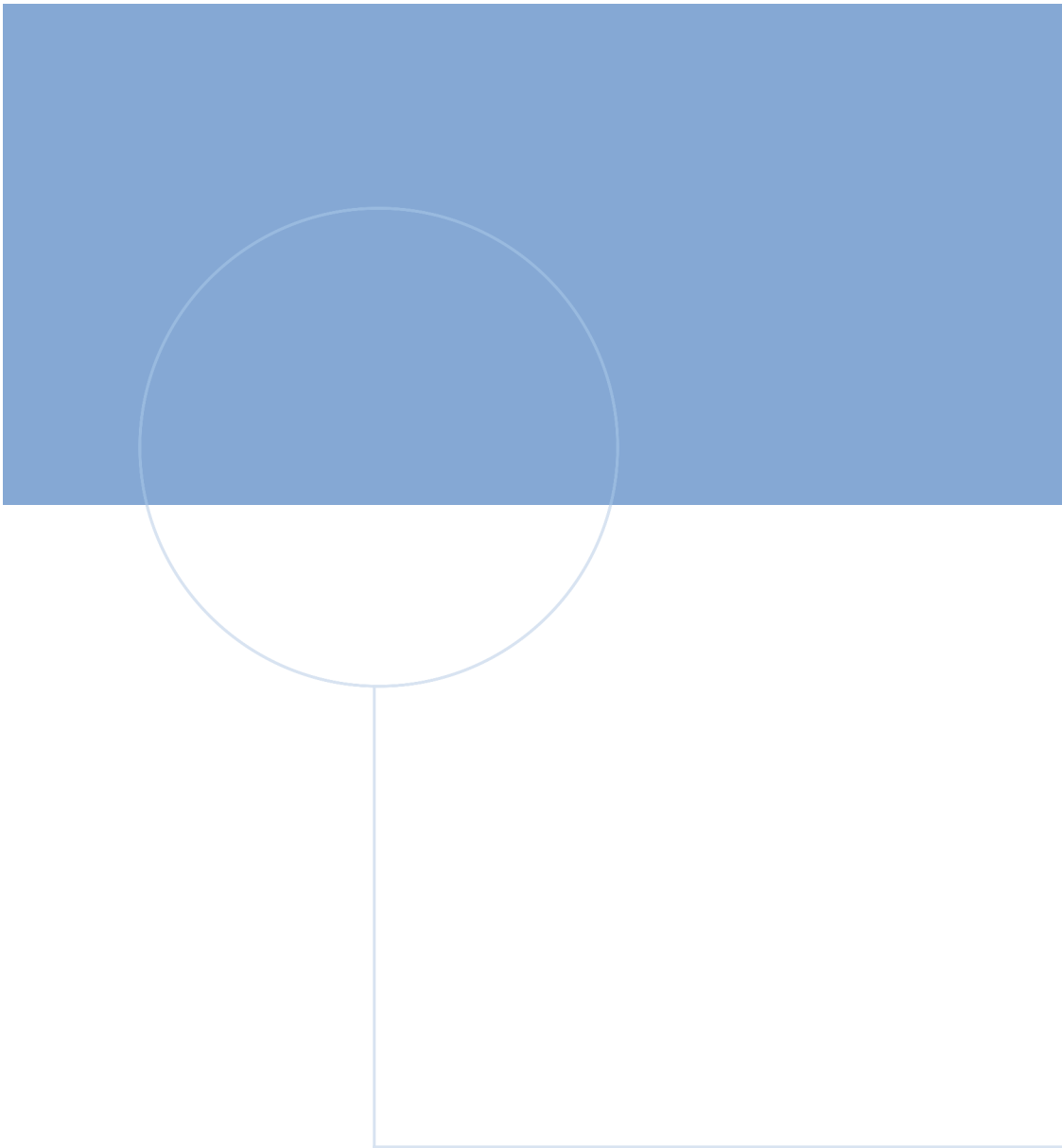

NTNU
Norwegian University of
Science and Technology